DALTON
FULL PAPER

Red and blue luminescent metallo-supramolecular coordination polymers assembled through π–π interactions †

Nathaniel W. Alcock,[a] Philip R. Barker,[a] Johanna M. Haider,[b]‡ Michael J. Hannon,*[a] Claire L. Painting,[a] Zoe Pikramenou,*‡[b] Edward A. Plummer,[a] Kari Rissanen[c] and Pauli Saarenketo[c]

[a] *Centre for Supramolecular and Macromolecular Chemistry, Department of Chemistry, University of Warwick, Coventry, UK CV4 7AL. E-mail: M.J.Hannon@warwick.ac.uk*
[b] *Department of Chemistry, University of Edinburgh, King's Buildings, West Mains Road, Edinburgh, UK EH9 3JJ*
[c] *Department of Chemistry, University of Jyväskyla, FIN-40351 Jyväskyla, Finland*

Received 1st January 2000, Accepted 13th March 2000

The use of π-stacking interactions to control the aggregation of photo-active metal centres is explored through the design of bis(2,2′;6′,2″-terpyridyl) metal complexes functionalised with biphenyl 'tails'. Aryl–aryl interactions control the aggregation of the metal complexes into polymetallic arrays in the solid state. Cobalt(II), ruthenium(II), nickel(II), copper(II), zinc(II) and cadmium(II) bis-ligand complexes and a mixed ligand ruthenium(II) complex have been structurally characterised. The solid-state structures are dependent on which units dominate the π-stacking. For cobalt, ruthenium, nickel and copper, biphenylene–biphenylene interactions lead to linear rod-like arrays, while for the group 12 d^{10} ions zinc and cadmium, biphenylene–pyridyl interactions lead to two-dimensional sheets. The addition of the biphenylene tail has favourable effects on the photophysical-properties of the complexes which exhibit room temperature red (ruthenium) or blue (zinc and cadmium) luminescence, both in solution and the solid state.

Introduction

The design of linear and branched (dendritic) polynuclear coordination arrays has attracted considerable recent interest. In view of the exciting electrochemical and photophysical properties of polypyridyl metal complexes,[1] the construction of multi-metallic arrays containing polypyridyl centres has been a particular focus. Construction approaches have focused mainly on covalently-linked systems through which discrete oligomers of controlled nuclearity[2–6] or infinite polymers[7,8] may be generated. Such discrete polynuclear arrays are proposed as potential supramolecular devices, exhibiting properties such as light-harvesting and energy-funneling,[9] while polymeric systems have been used as novel polyelectrolytes which can be incorporated into devices.[7] These covalent systems generally require multi-step (often low-yielding) syntheses. Non-covalent (supramolecular) approaches to generate multimetallic arrays have received less attention and have centred primarily on the use of hydrogen bonding.[10–14] Heterobimetallic systems have been prepared by linking metal complexes through nucleic acids[10–13] and polymetallic arrays prepared through carboxylic acid dimerisation.[14] A drawback to the use of hydrogen-bonding interactions is the poor solubility often associated with the precursors. This is especially true for nucleic acids.

We reasoned that aryl–aryl (π-stacking) non-covalent interactions might offer an alternative means of controlling the assembly of photo-active metal centres. While such interactions have proved a powerful tool for linking organic molecules into crystal-engineered structures,[15] their combination with polypyridyl metal complexes has received scant attention.[16] Importantly, the introduction of aromatic residues onto the outside of polypyridyl complexes should not be detrimental to their redox and photophysical properties. Indeed introduction of a tolyl group confers both increased extinction coefficients and extended emission lifetimes on ruthenium(II) and platinum(II) terpyridyl complexes.[4,17]

Our design strategy, therefore, was to add poly-aryl 'tails' to the outside of metal complexes and to use the interactions between these tails to control the aggregation of the metal centres into polymetallic arrays. To investigate this approach we chose biphenylene units as our poly-aryl 'tails'. This extended aryl system is capable of acting as a self-recognition motif (forming aryl–aryl interactions with another biphenylene unit) without introducing the solubility problems associated with larger aryl systems, such as pyrene. While biphenyl–biphenyl interactions should not be strong enough to cause complex aggregation in solution (except at very high concentrations), they should be adequate to achieve directionally-controlled aggregation in the solid state. This property is desirable, as it permits the discrete units from which the solid-state polymer is comprised to be fully characterised by the usual array of solution techniques. In contrast, traditional crystal engineering is solely dependent on solid-state techniques (most usually X-ray crystallography) for characterisation. We have focused our initial studies on biphenyl-substituted complexes of the simple polypyridyl ligand 2,2′;6′,2″-terpyridine (tpy), since the coordination chemistry of the unsubstituted tpy ligand with metal dications is well established[18,19] and tpy-based polypyridyl ligands have been used extensively in metallo-supramolecular design. As enunciated by Constable,[3] in contrast to 2,2′-bipyridine, tpy complex formation does not introduce complications of chirality. We believe that the strategy developed herein may be extended to a wide variety of alternative metallo-supramolecular arrays.

† Electronic supplementary information (ESI) available: rotatable 3-D crystal structure diagrams in CHIME format, structure and packing diagrams for the Co, Cd, Zn and Ru complexes. See http://www.rsc.org/suppdata/dt/b0/b000871k

‡ *Current address*: School of Chemistry, The University of Birmingham, Edgbaston, Birmingham, UK B15 2TT. E-mail: Z.Pikramenou@bham.ac.uk

DOI: 10.1039/b000871k

This journal is © The Royal Society of Chemistry 2000

Table 1 250 MHz ^{1}H NMR chemical shift (δ) data for biptpy and other relevant ligands in $CDCl_3$ solution at 298 K

	H6	H5	H4	H3	H3′	H4′	Ha/b	H*o*/*m*	H*p*
biptpy	8.73	7.35	7.89	8.69	8.78		8.01, 7.74	7.67, 7.47	7.47
phtpy[a]	8.71	7.35	7.89	8.68	8.75			7.91, 7.48	7.48
tpy[a]	8.70	7.34	7.86	8.63	8.46	7.97			

[a] Ref. 21.

Results and discussion

Ligand preparation

The ligand biptpy was prepared using the Kröhnke approach.[20] Reaction of an equimolar amount of 2-acetylpyridine with 4-biphenylcarboxaldehyde in aqueous ethanolic base at 0 °C yielded a yellow precipitate of 1-(2′-pyridyl)-3-(4″-biphenyl)-2-propen-1-one in 95% yield. Reaction of the enone with one equivalent of *N*-{2-(2′-pyridyl)-2-oxoethyl}pyridinium iodide[20] in ethanol in the presence of ammonium acetate afforded a deep green precipitate, which was purified by recrystallisation from ethanol in the presence of activated charcoal to give biptpy as an off-white solid in 42% yield.

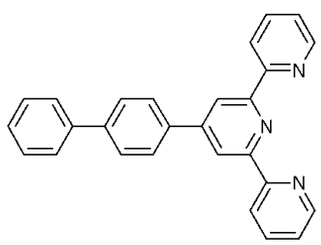

biptpy

The IR spectrum of biptpy reveals strong absorptions in the region 1600–1500 cm^{-1}, corresponding to aromatic stretches, and the lack of carbonyl peaks confirms the absence of starting materials. The FAB mass spectrum of biptpy shows a single peak corresponding to [M + 1] and microanalytical data is consistent with the proposed formulation. The ^{1}H NMR spectrum of biptpy in $CDCl_3$ solution has been recorded and the chemical shift data is tabulated in Table 1, together with the data for the related ligands tpy and 4′-phenyl-2,2′ : 6′,2″-terpyridine (phtpy). The ^{1}H NMR spectrum of biptpy indicates that the ligand is symmetrical on the NMR time-scale and is readily assigned from the distinctive splitting patterns of the pyridyl resonances and the splitting patterns, coupling constants and roofing patterns of the biphenylene protons; the spectral assignment has been confirmed by a COSY experiment. Comparison with the data for the unsubstituted tpy ligand[21] reveals that the presence of the substituent causes the proton adjacent to the site of substitution (H$^{3'}$) to shift downfield by 0.32 ppm, but the other pyridyl resonances are essentially unaffected. This downfield shift is anticipated for an adjacent aryl substituent and a very similar shift is observed in the spectrum of phtpy.[21]

Transition metal complex formation

Heating methanolic solutions containing two equivalents of biptpy with one equivalent of the acetate salts of cobalt(II), nickel(II), zinc(II), cadmium(II) or copper(II), or with the sulfate salt of iron(II), produced the complex cations $[M(biptpy)_2]^{2+}$ which were isolated as their hexafluorophosphate salts in 69–79% yield on treatment with ammonium hexafluorophosphate. The corresponding tetrafluoroborate salts could be obtained through treatment with ammonium tetrafluoroborate. Two ruthenium(II) complexes were prepared. Reaction of $[Ru(tpy)Cl_3]$ with biptpy in methanol in the presence of 4-ethylmorpholine, followed by treatment with methanolic ammonium hexafluorophosphate afforded the mixed ligand complex $[Ru(tpy)(biptpy)][PF_6]_2$ in 59% yield. Reaction of biptpy with ruthenium(III) trichloride in ethanol afforded $[Ru(biptpy)Cl_3]$ as a brown solid, which was reacted crude with a further equivalent of biptpy in methanol in the presence of 4-ethylmorpholine. Treatment of this solution with ammonium hexafluorophosphate afforded $[Ru(biptpy)_2][PF_6]_2$ as a red solid in 62% yield. Both of these ruthenium(II) complexes may also be isolated as their chloride salts by treatment of the reaction mixtures with lithium chloride or tetrafluoroborate salts through treatment with ammonium tatrafluoroborate.

The IR spectra of all these transition metal complexes exhibit peaks corresponding to the coordinated ligand and to the hexafluorophosphate counter-ion and partial microanalytical data for the complexes are consistent with the proposed formulations. The FAB mass spectral data for the bis-ligand complexes are also consistent with the proposed $[M(biptpy)_2][PF_6]_2$ formulation; all the complexes exhibit strong peaks for the parent ion $[M(biptpy)_2(PF_6)]^+$ and, in most cases, peaks for the fragments $[M(biptpy)_2]^+$ and $[M(biptpy)]^+$ are also observed. In the case of the mixed ligand complex $[Ru(biptpy)(tpy)][PF_6]_2$, peaks corresponding to $[Ru(biptpy)(tpy)(PF_6)]^+$, $[Ru(biptpy)(tpy)]^+$, $[Ru(biptpy)]^+$ and $[Ru(tpy)]^+$ are observed.

Solid-state structures

Background. Given the nature of our molecular design and the goal of designing non-covalently linked coordination polymers it is pertinent to consider how substituted and unsubstituted metal bis-terpyridyl complexes are normally arranged in the solid state. A survey of the Cambridge Crystallographic Database revealed a common packing motif for unsubstituted metal terpyridyl complexes $[M(tpy)_2]^{n+}$. The cations pack together through short face–face and edge–face aromatic–aromatic interactions between the terminal terpyridyl rings (centroid–centroid distances: face–face 3.5–4.1 Å; face–edge 4.9–5.3 Å. Face–edge interactions are often also termed aromatic CH $\cdots$ π interactions). This gives rise to sheets of interlocked cations (Fig. 1). Layers of anions are located between the sheets. Since an almost identical database survey has recently been reported in detail by Dance *et al.*[22] for unsubstituted terpyridyl complexes, further extensive description is unnecessary.

The introduction of substituents can disturb this packing motif; the interlocked sheet motif is maintained when small substituents (such as a catechol group)[23] are introduced at the 4′-position on the back of the terpyridyl central ring, but disrupted by large substituents. When a crown ether is attached to this 4′-position, the bis(terpyridyl)ruthenium(II) structure reveals only a one-dimensional chain containing such π–π contacts.[24] These tpy–tpy π–π interactions are completely absent from the structure of a bis(terpyridyl)cobalt(II) complex bearing bulky 4′-biphenylphosphine oxide substituents.[25] π–π interactions between substituents on the terpyridine are rare, although a tolyl–tolyl interaction has been described in a planar platinum(II) complex of 4′-tolyl-2,2′;6′,2″-terpyridine.[26]

To investigate the effect of a biphenyl substituent on the tpy–tpy packing motif and to introduce a new motif based on biphenyl–biphenyl interactions, we have investigated the crystal structures of seven of the complexes described herein. Although we have obtained all of the complexes described in a

crystalline form, the remainder have not yielded X-ray quality crystals.

Crystallographic investigations

Cobalt(II) complex. Red crystals of the complex $[Co(biptpy)_2][PF_6]_2$ were obtained from an acetonitrile solution by the slow diffusion of a diethyl ether–thf mixture and proved suitable for X-ray analysis.

The structure confirms the anticipated bis-ligand formulation of the complex cation. Intermolecular face–face aryl interactions between the biphenyl tails link the cations into infinite one-dimensional chains (Fig. 2). The two biphenyl rings and the central pyridyl to which they are attached stack with the equivalent three rings on an adjacent molecule, such that outer biphenyl rings stack with central pyridyl rings (4.29 Å centroid–centroid) and inner biphenyl rings stack with an adjacent inner biphenyl ring (4.22 Å centroid–centroid). This type of stacking is illustrated schematically in Fig. 3 as type A. Each pair of rings is approximately coplanar and offset. The planes of the rings are separated by *ca.* 3.7 Å. The one-dimensional chains are packed together into a two-dimensional plane (Fig. 2), however, no short aryl–aryl interactions (either face–face or face–edge) are observed between the chains.[27] The hexafluorophosphate anions and tetrahydrofuran solvent molecules are located between the planes containing the cation chains and form short contacts to protons in the planes above and below (ten H···F contacts in the range 2.49–2.20 Å). The chains stretch in the same direction in each plane and there are no short contacts between the two cation planes.[27]

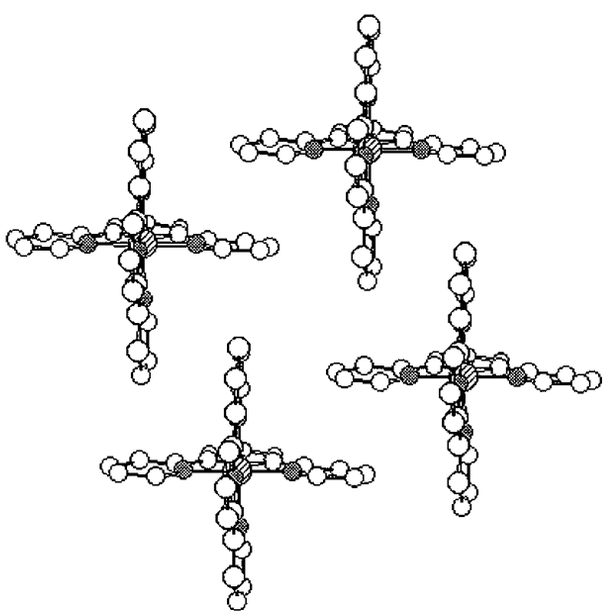

Fig. 1 Stacking motif observed in complexes of unsubstituted 2,2′;6′,2″-terpyridine; hydrogens omitted for clarity.

Thus, in this complex, we observe that the introduction of the biphenylene tails completely disrupts the tpy–tpy packing motif, observed with unsubstituted tpy ligands, and replaces it with tail–tail stacking interactions which aggregate the cations into one dimensional wire-like chains.

The cobalt(II) occupies a distorted octahedral geometry, coordinating to two terdentate ligands which each occupy three *mer* coordination sites (Fig. 2). The cobalt–nitrogen bond lengths to the central ring [1.873(11)–1.894(11) Å] are shorter than those to the terminal rings [1.925(11)–1.971(13) Å]. This arises from the constrained bite of this terdentate ligand: a similar pattern is observed in complexes of 2,2′:6′,2″-terpyridine with a range of different metals ions,[18,19] although, for this d^7 metal ion, the possibility of a Jahn–Teller contribution to the distortion cannot be excluded. A number of crystal structures of the unsubstituted $[Co(tpy)_2]^{2+}$ cation with different counter-ions have been reported.[28–33] Such cobalt(II) terpyridyl systems exhibit temperature-dependent spin-crossover behaviour and this influences the metal–ligand bond lengths. The structure of $[Co(biptpy)_2][PF_6]_2$ was obtained at low tem-

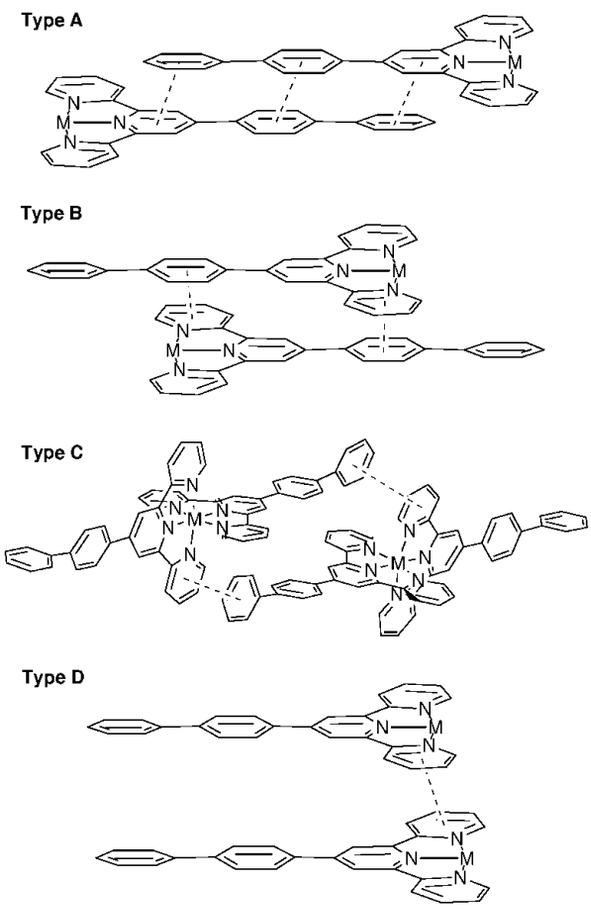

Fig. 3 Stacking motifs observed in the complexes of biptpy ligands.

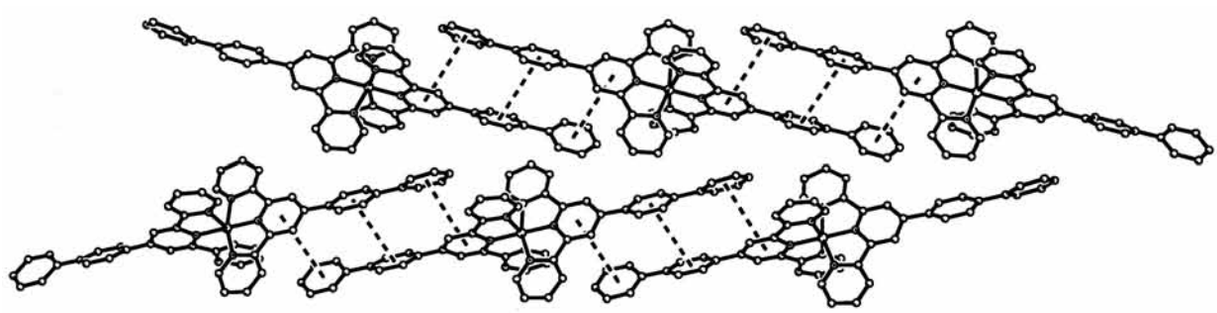

Fig. 2 Structure of the cation chains in the complex $[Co(biptpy)_2][PF_6]_2$; hydrogens omitted for clarity. Analogous cation chains are observed with ruthenium(II), nickel(II) and copper(II).

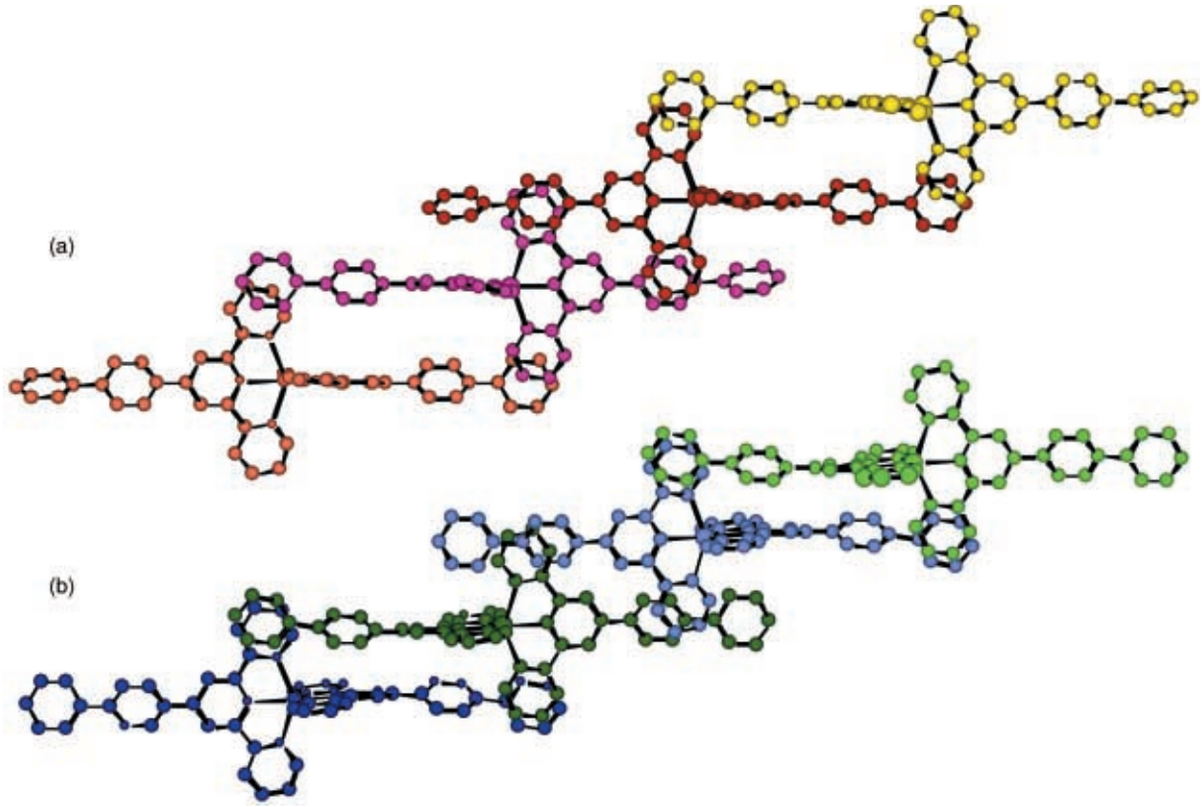

Fig. 4 Structure of the cation chains in the complex $[Cd(biptpy)_2][PF_6]_2$: (a) cation **1**; (b) cation **2**; hydrogens omitted for clarity.

perature (180 K) and the observed Co–N bond lengths [1.873(11)–1.971(13) Å] are significantly shorter than those of $[Co(tpy)_2][NO_3]_2 \cdot 2H_2O$ where the Co(II) centre is high spin[28] [2.075(5)–2.189(3) Å]. The terpyridyl units are approximately planar (torsion angles between rings 1.0–6.1°). The phenyl rings are twisted with respect to the adjacent rings about the interannular C–C bond by 23.5–43.3°; this is slightly larger than observed in related systems[34] and could be due to the crystal packing. The twist between the tpy unit and the inner phenyl ring (31.6, 43.3°) is greater than that between the two phenyl rings (23.5, 33.6°).

Ruthenium(II) complex. Red crystals of the complex $[Ru(biptpy)_2][BF_4]_2$ were obtained from a nitromethane solution by the slow diffusion of diethyl ether. The packing of this ruthenium bis-ligand complex is analogous to that in the cobalt(II) complex with type A three-ring face–face stacking interactions through the tail units leading to chains of cations. The outer biphenyl rings again stack with central pyridyl rings (4.20 and 3.99 Å centroid–centroid) and inner biphenyl rings stack with an adjacent inner biphenyl ring (3.82 Å centroid–centroid). The π–π separations are comparable with, though slightly shorter than, those observed in the cobalt complex. Again, the one-dimensional chains are packed together into a two-dimensional plane and the anions and solvent molecules reside between the planes. Thus, in this ruthenium(II) complex, the biphenylene tails again behave as effective assembly motifs, aggregating the cations into one- dimensional wire-like non-covalent chains.

The ruthenium(II) occupies a distorted octahedral geometry, coordinating to two terdentate ligands which each occupy three *mer* coordination sites. The ruthenium–nitrogen bond lengths to the central ring [1.978(3)–1.980(3) Å] are shorter than those to the terminal rings [2.063(3)–2.081(3) Å] and the bond lengths and angles are comparable with those observed in other ruthenium(II) terpyridyl systems.[21,24,25,35] The terpyridyl units are approximately planar (torsion angles between rings 1.5–7.5°) and the phenyl rings are twisted with respect to the adjacent rings about the interannular C–C bond by 27.2–37.1°. The twist between the tpy unit and the inner phenyl ring (36.3, 37.1°) is again greater than that between the two phenyl rings (27.2, 32.8°).

Copper(II) and nickel(II) complexes. Slow diffusion of diethyl ether into an acetone solution of the nickel(II) complex $[Ni(biptpy)_2][PF_6]_2$ yielded crystalline material, as did slow diffusion of benzene into a nitromethane solution of the copper(II) complex $[Cu(biptpy)_2][PF_6]_2$. Although these two complexes are not isomorphous with the cobalt or ruthenium complexes, they have very similar crystal packing. In each case, the anions and solvent molecules lie in channels between the cation planes and (for nickel and copper) are highly disordered. As a result their diffraction is very weak, which, with the difficulty of modelling the contents of the channels, leads to high conventional *R*-values. Despite this anion and solvent disorder, the cation geometries are well defined and the overall pattern of the packing is clear.

As indicated, the packing is analogous to that observed in the cobalt(II) and ruthenium(II) complexes (chains of cations linked by type A three-ring face–face stacking interactions through the central pyridyl and the two biphenyl rings), confirming that formation of chains through tail–tail interactions is a common motif for these d-block complexes. The face–face interactions are comparable with those in the cobalt(II) and ruthenium(II) complexes (copper complex: inner biphenyls 4.0–4.1 Å centroid–centroid; pyridyl/outer biphenyl 4.2–4.3 Å centroid–centroid; planes of the rings separated by *ca.* 3.7 Å. Nickel complex: inner biphenyls 3.9 Å centroid–centroid; pyridyl/outer biphenyl 4.3 Å centroid–centroid; planes of the rings separated by *ca.* 3.7 Å). The chains again pack into planes between which the anions and solvent molecules reside.

Cadmium(II) complex. Slow diffusion of benzene into a turquoise nitromethane solution of the cadmium complex $[Cd(biptpy)_2][PF_6]_2$ afforded pale purple crystals. The structure is illustrated in Fig. 4 and 5 and contains two crystallographically distinct cations (**1** and **2**). Both have the same basic

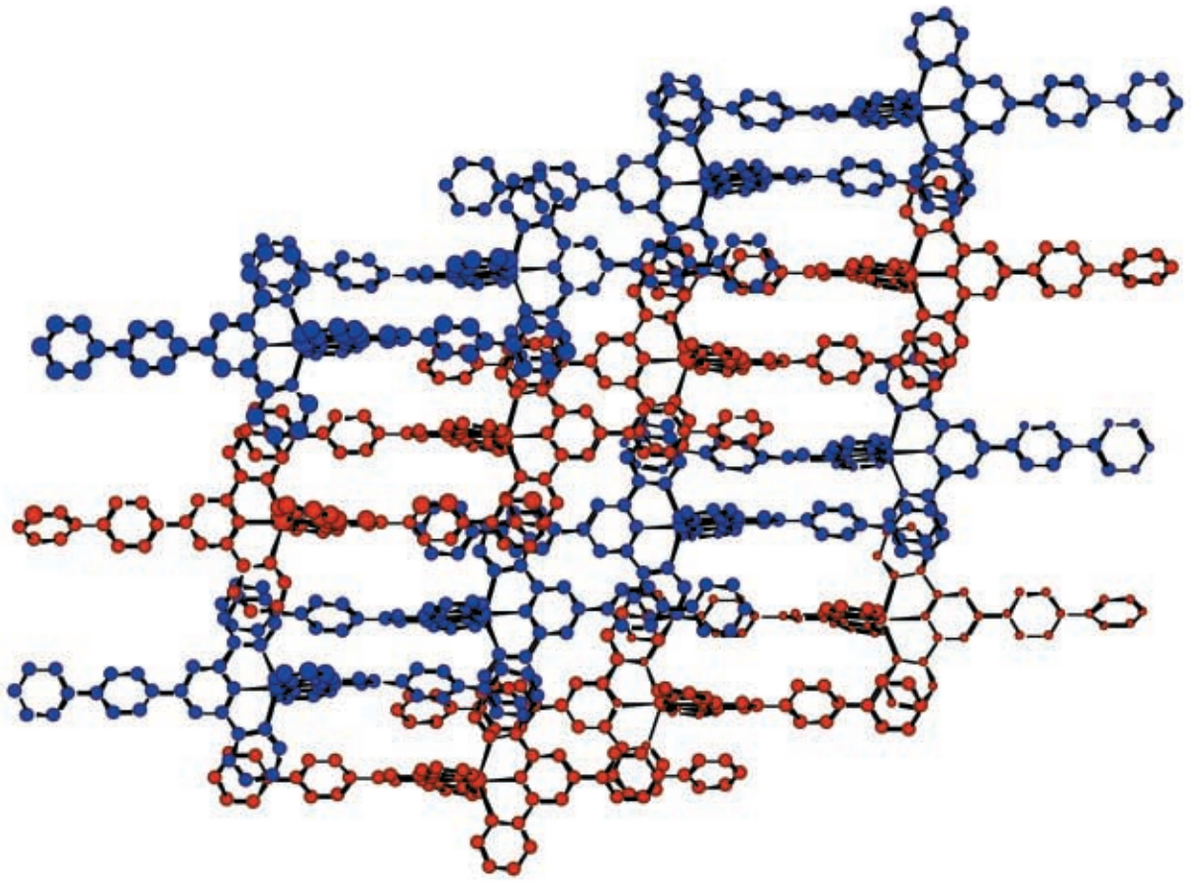

Fig. 5 Packing of the cation chains in the complex $[Cd(biptpy)_2][PF_6]_2$; hydrogens omitted for clarity. Red cation **1**, blue cation **2**.

structure and differ essentially only in the twisting of their biphenylene tails and the extent to which they form π-stacking interactions with other cations within the crystal.

The arrangement of these cations in the crystal lattice is quite different from that observed in the previous complexes and no three-ring (type A) stacks are observed between the biphenyl tails of the complex. Instead, the structure is dominated by interactions of types B and C (Fig. 3) in which a ring from the biphenyl tail stacks onto a terminal pyridyl ring.

These interactions lead to the formation of chains of cations and these are illustrated for the two types of cations in Fig. 4a and b. For cation **1** (Fig. 4a), one biptpy ligand forms an interaction of type B with another cation **1** resulting in two face–face π-interactions (centroid–centroid 4.01 Å, *e.g.* red–pink). These interactions lead to short contacts between the edge of the biphenyl ring and the face of a terminal pyridyl ring on the other coordinated biptpy ligand (centroid–centroid 5.13 Å; H···centroid 3.30 Å) and this may contribute to the interaction. At the other end of the complex, the second biptpy ligand interacts in a type C fashion with another cation **1** (centroid–centroid 3.99 Å, *e.g.* orange–pink). These two sets of interactions at either end of the cation lead to the chain structure. The chains containing the **2** cations are arranged in a similar fashion, although, as is evident in Fig. 4b, the face–face stacking is less effective and there are some face–edge (CH···π) contributions. For the type B interaction (centroid–centroid 4.28 Å, *e.g.* light blue–dark green), the rings are not coplanar but turned to give an H···centroid distance of 3.01 Å. This interaction also leads to the edge of the outer biphenyl ring stacking onto the face of a pyridyl ring on the other ligand (centroid–centroid 4.91 Å; H···centroid 2.87 Å). At the other end of the complex, there is a face–face type C interaction (centroid–centroid 4.16 Å, *e.g.* dark blue–dark green).

The two types of cation chains pack alongside each other to give a sheet containing alternate chains of cations **1** and **2** (Fig. 5). The chains are linked through face–face π-interactions between one pair of terminal pyridyl rings (centroid–centroid 3.84 Å: Fig. 3, type D interaction). This interaction is also associated with one face–edge π–π interaction (centroid–centroid 5.09 Å; H···centroid 2.95 Å). The other pair of terminal pyridyl rings, although coplanar, are distant (centroid–centroid 4.51 Å). Each cation thus forms only one set of short face–face interactions with one adjacent chain (*i.e.* these inter-chain links occur between any two chains only at every second cation). There are also face–edge links (through two rings) between two of the biphenyl tail units (centroid–centroid 4.63 and 4.24 Å; H···centroid 3.05 and 3.06 Å). The sheets also contain one nitromethane and one benzene solvent molecule for every two cations. The face of the benzene molecule stacks onto the edge of a pyridyl ring (centroid–centroid 4.89 Å; H···centroid 3.19 Å) while one of the methyl protons on the nitromethane forms a short contact with the faces of a pyridyl ring (H···centroid 3.12 Å). The hexafluorophosphate anions are also packed around the sheets and there are multiple short F···H contacts in the range 2.3–2.7 Å.

Each cadmium centre is 6-coordinate, bound to two terdentate biptpy ligands arranged in the anticipated *mer* configuration. The bond lengths to the central pyridyl ring [Cd–N 2.270(2)–2.290(3) Å] are shorter than those to the terminal pyridyl rings [Cd–N 2.322(3)–2.355(3) Å] as anticipated from the constrained tpy bite. Surprisingly, this appears to be the first crystallographically characterised cadmium(II) bis-complex of a terpyridyl ligand, however, these bond lengths are similar to those observed for other cadmium polypyridyl complexes.[36] The terpyridyl units are essentially planar (torsion angles 0.8–10.3°) and, as in the previously described complexes, the biphenyl tail rings are twisted (torsion angles: py–Ph 29.8–43.9°; Ph-Ph 30.5–36.6°).

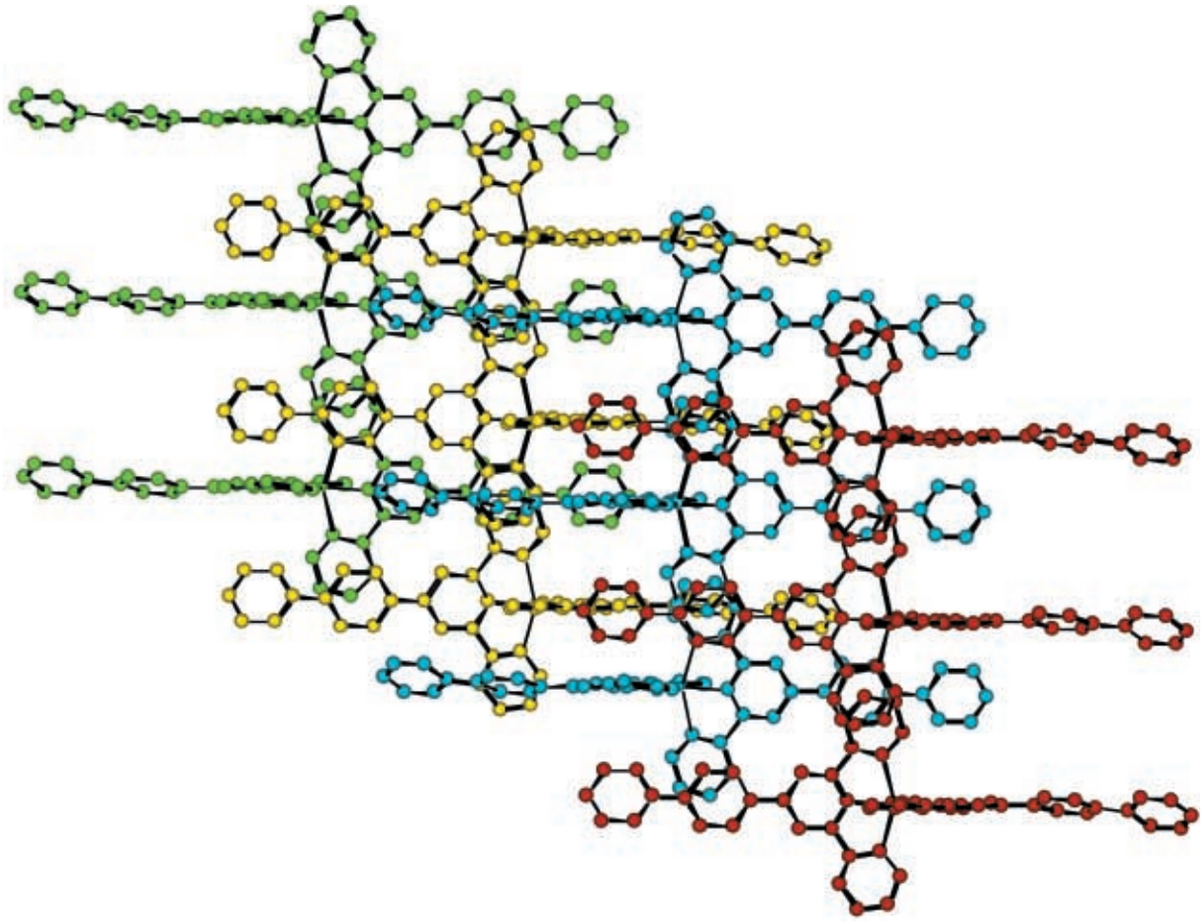

Fig. 6 Structure of the complex cation $[Zn(biptpy)_2]^{2+}$; hydrogens omitted for clarity.

Zinc(II) complex. Recrystallisation of the zinc(II) complex $[Zn(biptpy)_2][BF_4]_2$ from acetonitrile solution by slow diffusion of diethyl ether yielded colourless crystals. The structure reveals the anticipated $[Zn(biptpy)_2]^{2+}$ cations with zinc in a pseudo-octahedral coordination geometry encapsulated by two *mer*-coordinated biptpy ligands. The packing of these cations is again different from that of the cobalt, ruthenium, nickel and copper complexes, with no significant π-stacking interactions of type A between the biphenyl tails being observed. The structure shows similarities to the cadmium(II) complex but is slightly simpler, containing only type B and D (and no type C) interactions (Fig. 6).

Both biptpy ligands participate in type B interactions, forming two face–face π-stacking interactions with an adjacent molecule through a terminal pyridyl and the inner biphenyl ring (centroid–centroid 3.70 and 3.75 Å; *e.g.* yellow–green). These interactions are also associated with face–edge interactions (centroid–centroid 4.82 and 4.92 Å; H···centroid 2.76 and 3.09 Å) from the edge of biphenyl rings to the face of terminal pyridyl rings. These type B interactions lead to the formation of chains. Perpendicular to these chains, the terminal pyridyl rings of one set of biptpy ligands face–face π-stack with the terminal pyridyl rings on the adjacent chains (type D interaction; centroid–centroid 3.87 Å; *e.g.* green–green) aggregating the chains into a two dimensional sheet (Fig. 6). This face–face interaction is also associated with face–edge interactions (centroid–centroid 5.08 and 5.36 Å; H···centroid 3.06 and 3.17 Å) from the edge of one of the pyridyl rings in the face–face stack to a terminal pyridyl ring on the other biptpy ligand on the adjacent complex.

In this manner, two dimensional sheets are produced in which, as in the cadmium(II) structure, the biphenyl tails of the cations are all oriented along the same axis in the crystals. Solvent molecules (two acetonitriles per cation) and the tetrafluoroborate counter-ions are packed around the sheets. Some short face–edge contacts are observed between the sheets (centroid–centroid 4.96 and 5.41 Å; H···centroid 3.39 and 3.13 Å).

As anticipated, the zinc–nitrogen bond lengths to the central ring [2.066(3) and 2.077(3) Å] are shorter than those to the terminal rings [2.174(3)–2.194(3) Å]. The bond lengths and angles [75.51(11)–75.91(91)°] are unremarkable and comparable with those previously reported for bis-ligand zinc(II) complexes of terpyridyls bearing 3,4-dihydroxyphenyl and 3,4-dimethoxyphenyl groups in the 4′-position.[23] The terpyridyl units are approximately planar (Py–Py torsion angles 4.4–8.7°) as is expected and the interannular twists in the biphenyl tails (torsion angles; py–Ph 2.5 and 16.9°; Ph–Ph 17.5 and 28.1°) are smaller than those observed in the other structures.

The observed crystal structures of these bis-ligand metal dication complexes are thus divided into two classes. For cobalt(II), ruthenium(II), nickel(II) and copper(II) the biphenyl–biphenyl interaction envisaged in the design (type A) dominates and results in the formation of one-dimensional wire-like coordination polymers. The tpy–tpy (type D) interactions seen in the complexes of tpy ligands with small or no substituents[22] are not present. However, for the d^{10} metal ions zinc(II) and cadmium(II) this D-type interaction, coupled with tpy–biphenyl interactions (types B and C), leads to alternative structures containing two-dimensional sheet-like polymeric networks of metal centres. These two different classes of structure must be similar energetically and we speculate that more extended aryl substituents may drive the structure into a wire-like polymer for all metal ions. Clearly the electronic nature of the metal centre will influence the energy of the σ- and π-orbitals of the bound terpyridyl ligand (and hence the energetics of any tpy–tpy interactions), however, this is likely to be a subtle effect and difficult to quantify (although

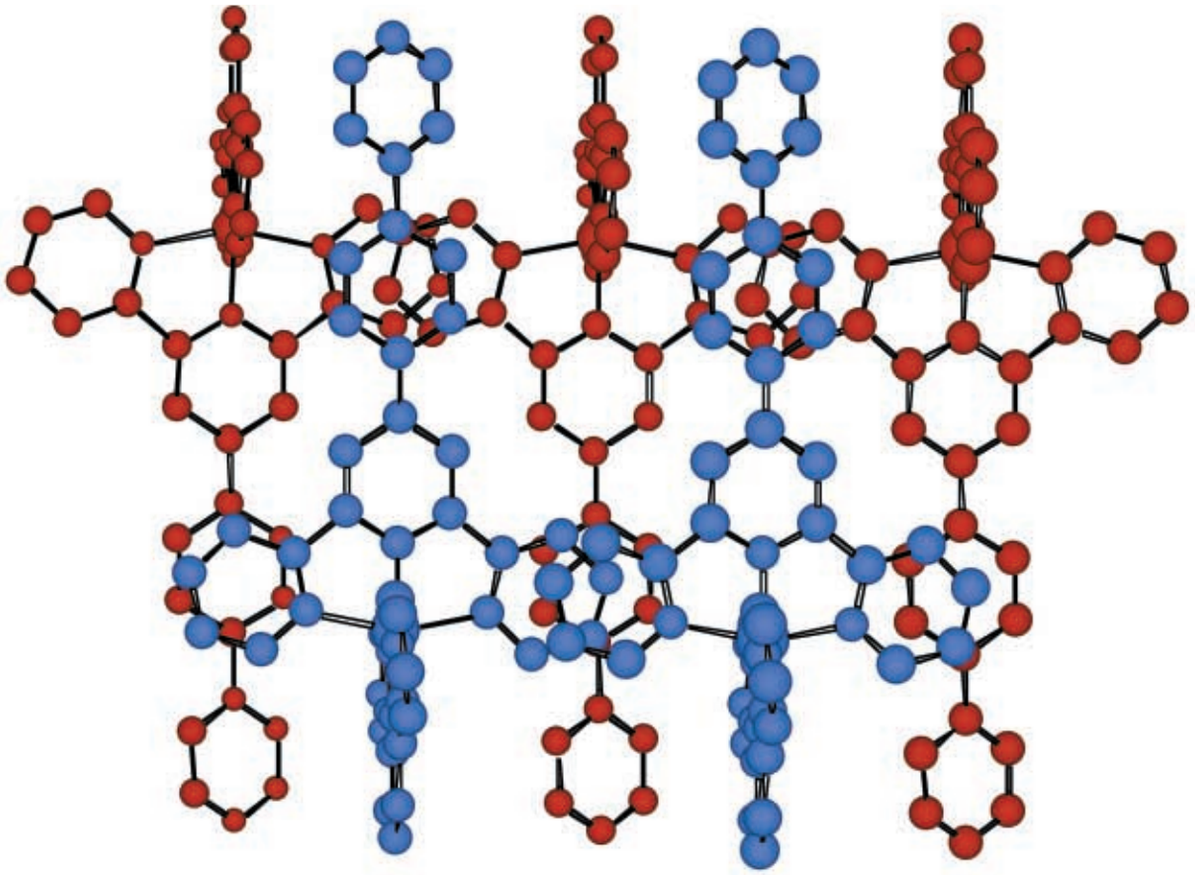

Fig. 7 Structure of the complex cation $[Ru(biptpy)(tpy)]^{2+}$; hydrogens omitted for clarity.

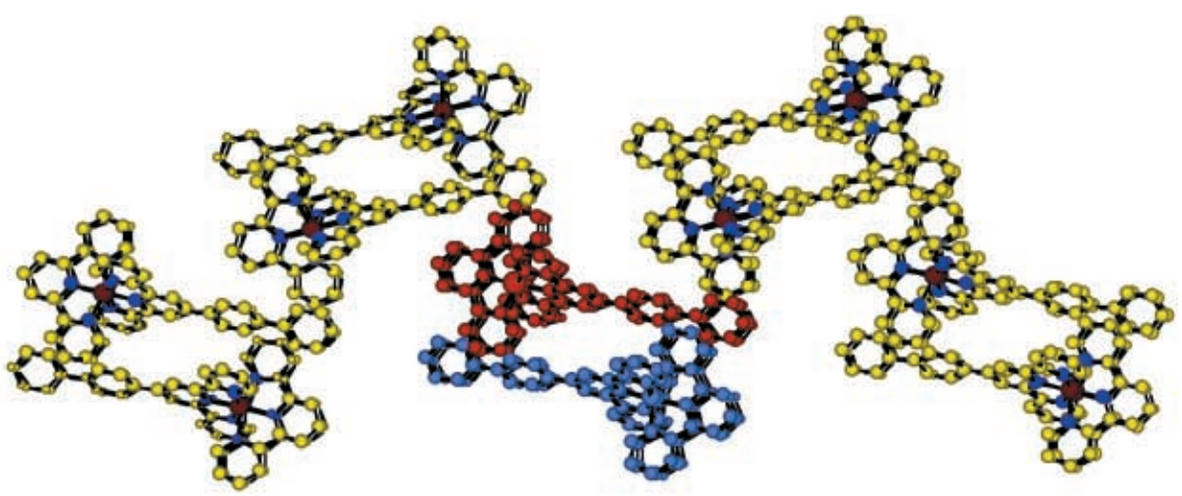

Fig. 8 Packing of the complex cation $[Ru(biptpy)(tpy)]^{2+}$ illustrating the formation of a network; hydrogens omitted for clarity.

it might explain why the second class of structures were observed with d^{10} metal centres).

Ruthenium(II) mixed ligand complex. The structure adopted by the mixed ligand complex $[Ru(tpy)(biptpy)]^{2+}$ is of interest, since it contains only one biphenyl tail unit per cation. Given the similar energetics of the two possible classes of structure when *two* biphenyl units are attached to each complex, for this mixed ligand cation bearing only one biphenyl substituent per complex, we would expect a structure similar to the second type (with type B/C and D interactions) to be favoured.

Red crystals of the mixed ligand complex $[Ru(tpy)(biptpy)]Cl_2$ were obtained by slow evaporation of a methanol solution of the complex. The crystals were of poor quality, giving weak diffraction. There is considerable anion and solvent disorder, however, the structure clearly reveals the cations and their solid-state packing.

The extended type A, face–face π-stacking between biphenylene tails is not observed for this complex. Instead, the structure is indeed a three-dimensional network dominated by pyridyl–pyridyl and pyridyl–biphenyl interactions (Fig. 7 and 8). Perhaps unsurprisingly, the biptpy ligand engages in more extensive π-stacking than the tpy ligand. The terminal pyridyl rings of the biptpy face–face π-stack (3.7 Å centroid–centroid) onto terminal pyridyl rings of the biptpy ligands of adjacent complexes in a type D interaction (Fig. 7; see, for example, the red cations). This leads to a one-dimensional chain. Each of these face–face stacking interactions is also associated with two face–edge π-interactions from the edge of the terminal pyridyl rings of the biptpy ligands to the face of a terminal pyridyl of

Table 2 250 MHz ^{1}H NMR chemical shift (δ) data for $[M(biptpy)_2][PF_6]_2$ (M = Fe, Ru, Zn and Cd) in CD_3CN solution at 298 K and related complexes

	H6	H5	H4	H3	H3′	H4′	Ha/b	H*o*/*m*	H*p*
$[Fe(biptpy)_2][PF_6]_2$	7.23	7.11	7.91	8.65	9.26		8.43, 8.12	7.91, 7.53	7.53
$[Fe(tpy)_2][BF_4]_2$ [a]	7.06	7.06	7.88	8.46	8.91	8.40			
$[Fe(phtpy)_2][PF_6]_2$ [a]	7.19	7.09	7.91	8.61	9.12			8.32, 7.82	7.74
$[Ru(biptpy)_2][PF_6]_2$	7.46	7.20	7.97	8.70	9.09		8.32, 8.05	7.86, 7.52	7.52
$[Ru(biptpy)(tpy)][PF_6]_2$	7.35	7.17	7.96	8.66	9.06		8.32, 8.06	7.86, 7.59	7.50
	7.43	7.17	7.92	8.50	8.75	8.41			
$[Ru(tpy)_2][PF_6]_2$ [a]	7.35	7.15	7.90	8.50	8.75	8.40			
$[Ru(phtpy)_2][PF_6]_2$ [b]	7.43	7.18	7.95	8.64	9.01			8.21, 7.75	7.75
$[Zn(biptpy)_2][PF_6]_2$	7.85	7.42	8.19	8.75	9.05		8.33, 8.05	7.85, 7.61	7.61
$[Cd(biptpy)_2][PF_6]_2$	8.10	7.55	8.23	8.80	9.01		8.28, 8.03	7.85, 7.55	7.55

[a] Ref. 37. [b] Ref. 36.

an unsubstituted terpyridyl ligand on the adjacent complex (4.9, 5.0 Å centroid–centroid). The complexes in the chain below are rotated through 180° permitting a series of inter-chain face–face π-stacking interactions (3.75 Å centroid–centroid; *e.g.* between blue and red cations) of type B between terminal pyridyl rings of the biptpy and inner rings of the biphenylene tails. This therefore leads to linked pairs of cation chains (Fig. 8; see for example blue and red cations). From these pairs, outer biphenyl rings face–face π-stack with terminal rings on the unsubstituted terpyridyl ligands (3.6 Å centroid–centroid) of adjacent pairs (Fig. 8) in a pseudo-type C interaction, and a three-dimensional network results.

The stacking is less extensive for the unsubstituted tpy ligand, with no pyridyl–pyridyl face–face interactions being observed. In addition to the aforementioned face–face interaction with the outer ring of a biphenylene tail and face–edge interactions with the edges of biptpy pyridyl rings, one additional type of interaction is observed; a face–edge interaction from the edge of the inner ring of a biphenylene and the face of a tpy terminal pyridyl (5.15 Å centroid–centroid).

The individual cations have the anticipated structure, with both terdentate ligands coordinated in a *mer* fashion to a pseudo-octahedral ruthenium(II) centre. The aryl rings in the biphenylene tail are less twisted with respect to the pyridines than in most of the other structures reported herein. The inner ring is almost coplanar with the pyridine to which it is attached (torsion angle 7°), while the outer ring is twisted through a further 29° with respect to the inner. Although the smaller spatial requirements of the chloride anion (*cf.* hexafluorophosphate and tetrafluoroborate in the other structures described herein) may well influence the structure adopted, we have been unable to obtain suitable crystals with these larger anions.

Solution behaviour

The solid-state structures illustrate that the biphenyl group has indeed been effective at aggregating the discrete metal terpyridyl centres into polymeric solid-state arrays either with a one-dimensional wire-like structure or a two-dimensional sheet structure. The introduction of a conjugated biphenyl unit might also be expected to cause perturbations to the properties of the discrete metal complexes and to investigate this, the solution chemistry has been examined.

^{1}H NMR. The complexes $[M(biptpy)_2]^{2+}$ (M = Fe, Ru, Zn and Cd) are diamagnetic. The 250 MHz ^{1}H NMR spectra of these complexes in CD_3CN solutions at 298 K have been recorded and are assigned and tabulated in Table 2, together with the corresponding data for the iron(II) and ruthenium(II) complexes of tpy and phtpy.[37]

The spectra are sharp and well resolved and illustrate the high symmetry of the complexes on the ^{1}H NMR time-scale. As expected, on complexation, H^6 shows the most dramatic shift with respect to the free ligand as it is closest to the metal ion.

Table 3 400 MHz ^{1}H NMR chemical shift (δ) data for $[M(biptpy)_2][PF_6]_2$ (M = Co or Ni) and related complexes in CD_3CN solution at 298 K

	Pyridyl						Biphenyl
$[Ni(biptpy)_2][PF_6]_2$	135	74	67	44		13	11–0
$[Ni(tpy)_2][PF_6]_2$ [a]	135	75	71	44	19	14	
$[Co(biptpy)_2][PF_6]_2$	92	54	42	32		14	10–7
$[Co(tpy)_2][PF_6]_2$ [b]	99	57	47	34	22	9	

[a] Ref. 38. [b] Ref. 39.

The terminal pyridyl rings of each ligand in the $[M(biptpy)_2]^{2+}$ cations are clearly in very similar environments to the terminal rings in the corresponding $[M(tpy)_2]^{2+}$ cations. The biphenyl substituent causes the proton on the central pyridyl ring ($H^{3'}$) to shift with respect to the tpy complex, however, this shift is closely mimicked in phtpy complexes. For $[Cd(biptpy)_2]^{2+}$, the H^6 resonance is significantly broadened. This probably arises from coupling to the spin active cadmium; no distinct cadmium satellites were resolved but may be hidden under the adjacent resonances. The ^{1}H NMR spectrum of $[Ru(biptpy)(tpy)][PF_6]_2$ is more complicated due to the presence of the two different ligands, but is readily assigned by COSY and NOE experiments. The proton resonances are at comparable shifts to those in $[Ru(biptpy)_2][PF_6]$ and $[Ru(tpy)_2][PF_6]_2$. Serial NMR dilutions were performed on the complex $[Fe(biptpy)_2][PF_6]$ in CD_3OD solution, starting from a saturated methanolic solution. The positions and appearances of the proton resonances were unaltered, implying that the biphenyl tails do not cause solution aggregation at milli- and submillimolar concentrations.

The complexes $[M(biptpy)_2]^{2+}$ (M = Ni or Co) are paramagnetic. Nevertheless, the 400 MHz ^{1}H NMR spectra of the complexes at 298 K in CD_3CN solutions were recorded. The ^{1}H resonances are paramagnetically shifted and considerably broadened (coupling data is thus lost), but reasonably well resolved. The chemical shift (δ) data for the nickel(II) and cobalt(II) complexes of biptpy are tabulated, together with the data for the corresponding tpy complexes,[38,39] in Table 3. There are 5 resonances due to the terpyridyl unit. Comparison with the ^{1}H NMR spectra of the tpy complexes shows, as expected, that the resonances are at similar chemical shifts, as would be anticipated for a similar solution structure. It has not been possible to fully assign the spectra, but the number of environments suggests that the solution species are symmetrical on the NMR time-scale. Comparison of the spectral data of the complexes of tpy and biptpy reveals the absence of one proton in the complexes of biptpy ($H^{4'}$) and allows us to assign the multiplets in the 0–11 range as arising from the biphenyl protons. The small shifts of these biphenyl resonances is compatible with the position of these protons being remote from the paramagnetic centre.

Table 4 Electrochemical data for $[M(biptpy)_2][PF_6]_2$ in acetonitrile solution ($[NBu_4][PF_6]$ supporting electrolyte). Potentials (V) quoted *vs.* Fc/Fc^+

	M(II/III)	M(II/I)	Ligand based reduction(s)	
$[Co(biptpy)_2][PF_6]_2$	−0.16	−1.16	−1.98	
$[Co(phtpy)_2][PF_6]_2$ [a]	−0.16	−1.17	−1.99	
$[Co(tpy)_2][PF_6]_2$ [a]	−0.13	−1.18	−2.06	
$[Ru(biptpy)_2][PF_6]_2$	0.89		−1.58	−1.79
$[Ru(biptpy)(tpy)][PF_6]_2$	0.90		−1.58	−1.87
$[Ru(tpy)_2][PF_6]_2$ [b]	0.92		−1.67	−1.92
$[Ru(phtpy)_2][PF_6]_2$ [c]	0.90		−1.66	−1.92
$[Fe(biptpy)_2][PF_6]_2$	0.69		−1.63	−1.76
$[Fe(phtpy)_2][PF_6]_2$ [a]	0.67		−1.62	−1.74
$[Fe(tpy)_2][PF_6]_2$ [b]	0.77		−1.64	−1.82

[a] Ref. 40. [b] Ref. 41. [c] Ref. 21.

Table 5 Selected electronic absorption spectroscopic data for the complexes $[M(biptpy)_2][PF_6]_2$ (M = Ru, Fe and Co) in acetonitrile solutions unless otherwise indicated

	λ_{max}/nm (ε/cm^{-1} mol^{-1})
$[Ru(biptpy)_2][PF_6]_2$	494 (45 000)
$[Ru(biptpy)(tpy)][PF_6]_2$	484 (17 000)
$[Ru(tpy)_2][PF_6]_2$ [a]	474 (10 400)
$[Ru(phtpy)_2][PF_6]_2$ [a]	487 (26 200)
$[Fe(biptpy)_2][PF_6]_2$	571 (23 000)
$[Fe(phtpy)_2][PF_6]_2$ [b]	565 (22 600)
$[Fe(tpy)_2][PF_6]_2$ [b]	552 (11 900)
$[Co(biptpy)_2][PF_6]_2$	445 (3400), 518 (3000)
$[Co(tpy)_2][PF_6]_2$ [c]	415 (1500), 443 (1500), 503 (1200)
biptpy [d]	253 (74 000), 284 (13 000)
$[Cd(biptpy)_2][PF_6]_2$	236 (60 000), 285 (59 000), 326 (70 000)
$[Cd(biptpy)_2][PF_6]_2$ [d]	233 (37 000), 286 (46 000), 322 (36 000)
$[Zn(biptpy)_2][PF_6]_2$ [d]	238 (67 000), 285 (63 000), 336 (83 000)

[a] Ref. 42. [b] Ref. 40. [c] Ref. 43. [d] In methanol solution.

Electrochemistry. The electrochemical behaviour of some of the salts $[M(biptpy)_2][PF_6]_2$ (M = Co, Ru, Fe, Cu and Ni) in acetonitrile solution was investigated by cyclic voltammetry. The results are summarised in Table 4, together with the corresponding data for the cobalt(II), ruthenium(II) and iron(II) tpy and phtpy complexes.[21,40,41] As would be expected, the biphenyl substituent has little effect on the metal-based redox chemistry, however all the ligand-based reductions are slightly lower in energy, due to the increase in conjugation within biptpy in comparison to tpy.

Cyclic voltammetry on the nickel(II) and copper(II) complexes is less informative: In the cyclic voltammetric spectrum of $[Ni(biptpy)_2][PF_6]_2$, an irreversible reduction process at −0.85 V and an irreversible terpyridyl-centred reduction at −1.85 V are observed. For $[Cu(biptpy)_2][PF_6]_2$, an irreversible reduction process is observed at −0.44 V with an associated absorption spike at −0.67 V. This is due to copper(0) plating on the electrode. An irreversible terpyridyl-centred reduction is also observed at −1.87 V. In both cases, the complexes of the unsubstituted tpy ligand behave in a similar fashion.

Absorption spectra. The absorption spectra were recorded for acetonitrile solutions of the complexes $[M(biptpy)_2][PF_6]_2$ (M = Co, Ru, and Fe). Selected wavelengths of the peaks and absorption coefficients are given in Table 5. Data for $[M(tpy)_2][PF_6]_2$ and $[M(phtpy)_2][PF_6]_2$ complexes are also shown for comparison.[40,42,43]

As observed in the electrochemistry, the energy of the ligand π* is lowered with respect to terpyridine in the more conjugated biptpy ligand. Consequently, the MLCT bands of these biptpy complexes are shifted to higher wavelength when compared to the corresponding tpy complexes. For $[Ru(biptpy)(tpy)][PF_6]_2$, two distinct MLCT bands might be expected, however, as a result of the broad nature of the bands and their relatively small wavelength separation, a single broad peak is observed centred between the expected positions of the two bands.

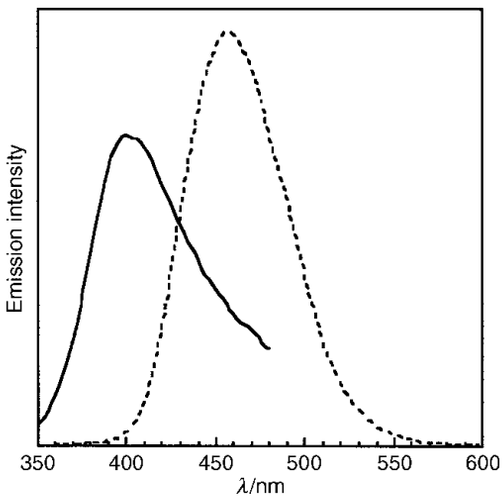

Fig. 9 Emission spectra of $[Zn(biptpy)_2][PF_6]_2$ in the solid state using a powder sample (solid line) and in methanol solution (intermittent line). The samples were excited at 250 nm.

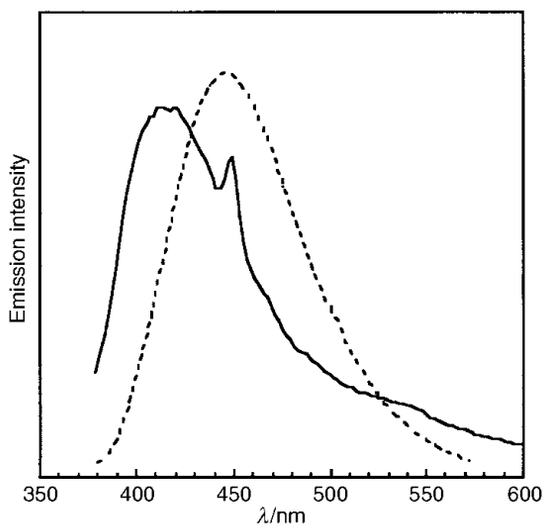

Fig. 10 Emission spectra of $[Cd(biptpy)_2][PF_6]_2$ in the solid state using a powder sample (solid line) and in methanol solution (intermittent line). The samples were excited at 250 nm.

Serial dilutions over the 10^{-3}–10^{-5} M concentration range were performed on the complex $[Fe(biptpy)_2][PF_6]$ in methanol solution and revealed no changes in peak maxima, shape or extinction coefficients which is consistent with an absence of solution aggregation and in agreement with the NMR observations.

Luminescence studies. The cadmium and zinc complexes show strong blue emission with high quantum yields when excited with UV light. The luminescence of the complexes in solution and the solid state are shown in Fig. 9 and 10. While the free ligand emits in the UV region of the spectrum (390 nm in MeOH and 395 nm in solid state), the emission of the complexes is considerably red-shifted and consequently, emission occurs in the visible blue region of the spectrum. The red-shift in one of the ligand-based absorption bands observed upon coordination is consistent with this. Coordination also enhances the quantum yield; in methanol solution the zinc complex emits with a quantum yield of 0.80, while the quantum yield for the cadmium complex is 0.71. These values are both higher than that for the ligand (0.55) under the same excitation

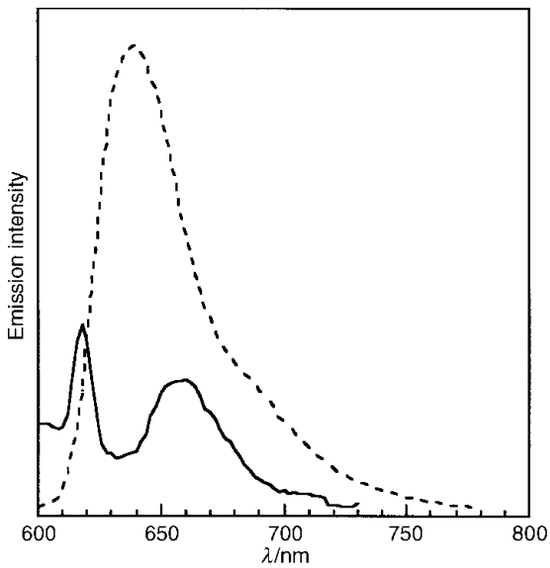

Fig. 11 Emission spectra of $[Ru(biptpy)_2][PF_6]_2$ in the solid state at room temperature (solid line) $\lambda_{exc} = 480$ nm and in degassed acetonitrile at 77 K (intermittent line) $\lambda_{exc} = 490$ nm.

conditions. The same emission wavelength is observed on excitation at 250 nm or in the lower energy absorption band at 330 nm. Blue luminescence has previously been reported from zinc complexes of other pyridyl-containing ligands and it is unsurprising that the zinc complex of the biphenyl terpyridine ligand employed in our studies exhibits similar behaviour.[44–46] The luminescence is usually attributed to intra-ligand ππ* transitions, with no reported shifts upon coordination, however, recently, involvement of charge transfer states in the case of aryl tpy ligands has been proposed.[46] Given that zinc(II) polypyridyl complexes are known emitters, it is perhaps surprising that emission from cadmium(II) polypyridyl complexes has not, to the best of our knowledge, been previously examined. For this biptpy ligand, the luminescence behaviour of the cadmium complex is similar to that of the zinc analogue.

The ability to design blue luminescent materials is desirable for display applications and to this end Che *et al.* have reported blue luminescence of solutions of some zinc pyridylamine complexes.[45,47] For the biptpy complexes, the high quantum yields of luminescence in solution (which are enhanced with respect to the free ligand) and the strong luminescence in the solid state, coupled with the potential to use supramolecular design to control and vary the solid-state structure, suggest that materials such as these merit exploration for application as blue light emitting diodes.

While ruthenium(II) complexes of bipyridyl ligands exhibit characteristic red luminescence from the ^{3}MLCT state, for the ruthenium(II) complex of tpy, this state is quenched by a low-lying ^{3}MC state and room temperature emission is not observed. Addition of simple donor and acceptor substituents at the 4′-position ligand alters the relative energies of these states and appropriate combinations can achieve luminescent behaviour in a predictable fashion.[42] For aryl substituents the situation is complicated by the potential for inter-aryl twisting in the ground and excited states. Nitrile solutions of bis(tolylterpyridine) complexes [but not bis(phenylterpyridyl) complexes] of ruthenium(II) exhibit weak room temperature luminescence.[4] Similarly, we observe that acetonitrile or aqueous solutions of the complex $[Ru(biptpy)_2]^{2+}$ prepared herein, exhibit weak red luminescence. In the solid state (powder) and in acetonitrile solution at low temperature the complex shows strong red luminescence on irradiation in the visible MLCT absorption band (Fig. 11).[48] The emission spectroscopic data for the ruthenium complexes, along with those for related compounds for comparison, are listed in Table 6.

Table 6 Emission spectroscopic data for the complexes $[Ru(biptpy)_2][PF_6]_2$, $[Ru(biptpy)(tpy)][PF_6]_2$ and related complexes

	λ_{em}(max)/nm		
	298 K	77 K in CH_3CN	Solvent
$[Ru(biptpy)_2][PF_6]_2$	640	634	MeCN
$[Ru(biptpy)_2]Cl_2$	640		H_2O
$[Ru(biptpy)(tpy)][PF_6]_2$	—	630	MeCN
$[Ru(tpy)_2][PF_6]_2$ [a]	—	598	MeCN
$[Ru(ttpy)_2][PF_6]_2$ [a]	640	628	MeCN
$[Ru(tpy)(ttpy)][PF_6]_2$ [b]		622	MeCN

[a] Ref. 4. [b] Ref. 49.

The complexes of this biptpy ligand therefore represent an example of classes of systems in which there is potential not only to create blue luminescent materials of controlled solid-state architecture but, through selection of the metal ion, to tune the luminescent properties of the material to achieve red luminescence also.

Conclusions

We have shown that addition of a biphenylene tail to a simple terpyridyl ligand permits the synthesis of complexes which exhibit red and blue luminescence in both solution and the solid state. The solid-state structures are dependent on which types of π-stacking interactions predominate. Biphenylene–biphenylene interactions lead to rod-like wire structures while biphenylene–pyridyl interactions lead to two-dimensional sheets. The strategy developed herein is currently being extended to other metallo-supramolecular architectures (such as boxes[49]) and the structural and photophysical effects of more extended aryl tails are being examined. Aside from their self-recognition properties, the aryl tails may also potentially be captured by cyclodextrin hosts and these complexes are being explored as part of ongoing studies aimed at employing cyclodextrin binding to construct non-covalent photo-active arrays.[50]

Experimental

General details

IR spectra were recorded on a Perkin-Elmer Paragon 1000 FT spectrophotometer at a resolution of 4 cm^{-1}, with the samples in the form of compressed KBr discs. Absorption spectra were recorded on Unicam 8700 and Jasco V550 spectrometers. ^{1}H NMR spectra were recorded on Brüker ACF250, DPX300 and ACP400 spectrometers. 2D sequences used standard Brüker software.[63] Electron impact (EI) mass spectra were recorded on a Micromass Autospec spectrometer. Fast atom bombardment (FAB) mass spectra were recorded using 3-nitrobenzyl alcohol as matrix on Micromass Autospec spectrometers either at Warwick or by the EPSRC National Mass Spectrometry Service Centre, Swansea. Microanalyses were conducted on a Leeman Labs CE44 CHN analyser by the University of Warwick Analytical Service. Electrochemical measurements were performed using an ecochimie Autolab electrochemical workstation using standard GPES software.[64] A conventional three-electrode configuration was used, with platinum working and auxiliary electrodes and a $Ag–Ag^+$ reference. The measurements were conducted in acetonitrile solution with 0.1 M $[Bu^n_4N][PF_6]$ base electrolyte. Potentials are quoted *vs.* ferrocene/ferrocenium couple ($Fc/Fc^+ = 0.0$ V), and all potentials were referenced to internal ferrocene added at the end of each experiment.

The luminescence studies were performed on a Quanta-Master QM-1 steady-state emission spectrometer from Photon Technology Instruments equipped with a 75 W xenon arc lamp and a model 810 photon counting detection system with a red-sensitive R928 photomultiplier tube. Single-grating monochromators are used for wavelength selection of the excitation light and the luminescence. The emission monochromator grating is blazed at 550 nm. The data were collected and analysed with Felix software.[65] The luminescence quantum yields of methanolic solutions of the complexes were measured using quinine sulfate in 0.01 N H_2SO_4 as a standard with quantum yield 0.54.[51] All the samples for the quantum yield measurements were excited at 250 nm to minimise excitation wavelength errors. An error value of 10% is associated with the quantum yield measurements.

Precious metal salts (Johnson Matthey) and other chemicals (Aldrich) were used as supplied. *N*-{2-(2′-Pyridyl)-2-oxoethyl}pyridinium iodide[20] and $[Ru(tpy)Cl_3]$[21] were prepared according to literature methods.

1-(2′-Pyridyl)-3-(4″-biphenyl)-2-propen-1-one

A solution of biphenyl-4-carboxaldehyde (1.50 g, 8.2 mmol) in ethanol (18 cm^3) was treated with a solution of sodium hydroxide (1 g, excess) in water (13 cm^3), and 2-acetylpyridine (0.9 cm^3, 8.2 mmol). The yellow mixture was stirred at 0 °C for 1 h. The yellow solid that precipitated was collected by vacuum filtration and washed with ice cold methanol (1.87 g, 59%). IR (KBr): *ν* 1670s, 1600s, 1484w, 1450m, 1334s, 1218s, 1033s, 998s, 836m, 759s, 674s cm^{-1}. MS (+ve FAB): *m*/*z* 286 [M + 1]. Found: C, 82.6; H, 5.2; N, 5.1. Calc. for $C_{20}H_{15}NO·0.25H_2O$: C, 82.9; H, 5.4; N, 4.8%. ^1H NMR ($CDCl_3$, 250 MHz, 298 K): *δ* 8.76 (1H, d, *J* = 4.6 Hz, H6), 8.33 (1H, d, *J* = 16.3 Hz, Hc/d), 8.19 (1H, d, *J* = 7.0 Hz, H3), 7.98 (1H, d, *J* = 16.0 Hz, Hc/d), 7.88 (1H, td, *J* = 7.9, 1.8 Hz, H4), 7.80 (2H, d, *J* = 8.4 Hz, H*o*/*m*/a/b), 7.64 (4H, dd, *J* = 8.4, 6.1 Hz, H*o*/*m*/a/b), 7.50 (4H, m, Hp,5,*o*/*m*/a/b).

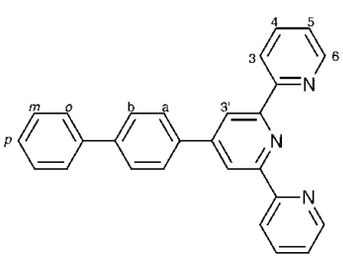

4′(4-Biphenyl)-2,2′:6′,2″-terpyridine (biptpy)

1-(2′-Pyridyl)-3-(4″-biphenyl)-2-propen-1-one (2.000 g, 7.0 mmol), *N*-{2-(2′-pyridyl)-2-oxoethyl}pyridinium iodide (2.282 g, 7.0 mmol) and ammonium acetate (5 g, excess) in ethanol (80 cm^3) were heated under reflux for 12 h. On cooling, a green solid precipitated and was collected by vacuum filtration and recrystallised from ethanol in the presence of activated charcoal to yield biptpy as an off-white solid (1.132 g, 42%). IR (KBr): *ν* 1591s, 1582s, 1538w, 1569m, 1442w, 1388s, 790s, 763s, 721m, 682m cm^{-1}. MS (+ve FAB): *m*/*z* 386 [M + 1]. Found: C, 83.3; H, 4.9; N, 10.8. Calc. for $C_{27}H_{19}N_3·0.25H_2O$: C, 83.2; H, 5.0; N, 10.8%. UV–Vis (MeOH): λ_{max} (*ε*) 253 (74 000), 284 (13 000 cm^{-1} mol^{-1}). ^1H NMR ($CDCl_3$, 250 MHz, 298 K): *δ* 8.78 (2H, s, H3′), 8.73 (2H, d, *J* = 4.7 Hz, H6), 8.69 (2H, d, *J* = 8.1 Hz, H3), 8.01 (2H, d, *J* = 8.4 Hz, Ha/b), 7.89 (2H, td, *J* = 7.6, 1.8 Hz, H4), 7.74 (2H, d, *J* = 8.7 Hz, Ha/b), 7.67 (2H, d, *J* = 7.0 Hz, H*o*/*m*), 7.47 (3H, m, H*p*,*o*/*m*), 7.35 (2H, ddd, *J* = 7.6, 4.9, 1.2 Hz, H5).

$[Fe(biptpy)_2][PF_6]$

Biptpy (0.0205 g, 0.05 mmol) and iron(II) sulfate (0.0074 g, 0.026 mmol) were heated to reflux in methanol (15 cm^3) for 12 h. The resulting purple solution was cooled and treated with saturated methanolic ammonium hexafluorophosphate. On cooling, a purple solid separated and was isolated by filtration (0.023 g, 78%). IR (KBr): *ν* 1616m, 1403m, 1122m, 844s cm^{-1}. MS (+ve FAB): *m*/*z* 441 [Fe(biptpy)], 826 $[Fe(biptpy)_2]$, 971 $[Fe(biptpy)_2(PF_6)]$. Found: C, 56.9; H, 3.4; N, 7.3. Calc. for $FeC_{54}H_{38}N_6·1.5H_2O$: C, 56.7; H, 3.6; N, 7.3%. UV–Vis (MeCN): λ_{max} (*ε*) 239 (36 000), 285 (48 000), 324 (61 000), 571 nm (23 000 cm^{-1} mol^{-1}). ^1H NMR (CD_3CN, 250 MHz, 298 K): *δ* 9.26 (2H, s, H3′), 8.65 (2H, d, *J* = 7.8 Hz, H3), 8.43 (2H, d, *J* = 8.7 Hz, Ha/b), 8.12 (2H, d, *J* = 8.4 Hz, Ha/b), 7.91 (4H, m, H*o*/*m*, 4), 7.53 (3H, m, H*o*/*m*,*p*), 7.23 (2H, d, *J* = 4.9 Hz, H6), 7.11 (2H, ddd, *J* = 8.7, 5.5, 1.2 Hz, H5). ^1H NMR (CD_3OD, 250 MHz, 298 K): *δ* 9.56 (2H, s, H3′), 8.93 (2H, d, *J* = 7.9 Hz, Ha/b), 8.56 (2H, d, *J* = 8.6 Hz, H3), 8.12 (2H, d, *J* = 8.7 Hz, Ha/b), 8.04 (2H, td, *J* = 8.4, 1.4 Hz, H4), 7.90 (1H, dd, *J* = 8.4, 1.5 Hz, H*o*), 7.59 (2H, t, *J* = 7.2 Hz, H*m*), 7.49 (1H, t, *J* = 7.2 Hz, H*p*), 7.38 (2H, d, *J* = 4.6 Hz, H6), 7.27 (2H, ddd, *J* = 8.1, 5.4, 1.2 Hz, H5).

The tetrafluoroborate was prepared in 73% yield in an analogous fashion, precipitating by addition of a saturated methanolic solution of ammonium tetrafluoroborate. The chloride salt was prepared in 84% yield from iron(II) chloride.

$[Co(biptpy)_2][PF_6]_2$

Biptpy (0.0201 g, 0.05 mmol) and cobalt(II) acetate (0.0064 g, 0.026 mmol) were heated to reflux in methanol (15 cm^3) for 12 h. The resulting red-coloured solution was cooled and treated with saturated methanolic ammonium hexafluorophosphate. A red precipitate separated and was isolated by filtration (0.020 g, 71%). The red precipitate was recrystallised from acetonitrile by the slow diffusion of diethyl ether containing tetrahydrofuran to afford red crystals of $[Co(biptpy)_2][PF_6]_2$. IR (KBr): *ν* 1616s, 836s, 767w, 559m, 466m cm^{-1}. MS (+ve FAB): *m*/*z* 444 [Co(biptpy)], 829 $[Co(biptpy)_2]$, 974 $[Co(biptpy)_2(PF_6)]$. Found: C, 57.4; H, 3.5; N, 7.3. Calc. for $CoC_{54}H_{38}N_6P_2F_{12}·0.5H_2O$: C, 57.5; H, 3.5; N, 7.4%. UV–Vis (MeCN): λ_{max} (*ε*) 236 (43 000), 284 (46 000), 324 (50 000), 445 (3400), 518 nm (3000 cm^{-1} mol^{-1}). ^1H NMR (CD_3CN, 400 MHz, 298 K): *δ* 92, 54, 42, 32, 14, 10–7.

The tetrafluoroborate salt was prepared in 83% yield in an analogous fashion, precipitating by addition of a saturated methanolic solution of ammonium tetrafluoroborate.

$[Ni(biptpy)_2][PF_6]_2$

Biptpy (0.0202 g, 0.05 mmol) and nickel(II) acetate (0.0065 g, 0.026 mmol) were heated to reflux in methanol (15 cm^3) for 12 h. The resulting green solution was cooled and treated with saturated methanolic ammonium hexafluorophosphate. On cooling, a green solid separated and was isolated by filtration (0.020 g, 69%). IR (KBr): *ν* 1616s, 1569w, 1546w, 1473s, 1427s, 1400m, 1384w, 1303w, 1245m, 1164w, 1018m, 833s, 794m, 767s, 732m, 701m, 659w, 559s cm^{-1}. MS (+ve FAB): *m*/*z* 443 [Ni(biptpy)], 973 $[Ni(biptpy)_2(PF_6)]$. Found: C, 56.3; H, 3.4; N, 7.0. Calc. for $NiC_{54}H_{38}N_6P_2F_{12}·2H_2O$: C, 56.1; H, 3.7; N, 7.3%. ^1H NMR (CD_3CN, 400 MHz, 298 K): *δ* 135, 74, 67, 44, 13, 11–0.

The tetrafluoroborate salt was also prepared, in 66% yield, in an analogous fashion by precipitating *via* addition of a saturated methanolic solution of ammonium tetrafluoroborate.

$[Cu(biptpy)_2][PF_6]_2$

Biptpy (0.0203 g, 0.05 mmol) and copper(II) acetate (0.0052 g, 0.026 mmol) were heated to reflux in methanol (15 cm^3) for 12 h. The resulting green solution was cooled and treated with saturated methanolic ammonium hexafluorophosphate. On cooling, a green solid separated and was isolated by filtration (0.023 g, 79%). IR (KBr): *ν* 1619s, 1573m, 1477s, 1427m, 1400w, 1384w, 1249m, 1164w, 1022m, 848s, 794w, 767m, 728w, 690w, 859w, 559s cm^{-1}. MS (+ve FAB): *m*/*z* 448 [Cu(biptpy)], 833 $[Cu(biptpy)_2]$, 978 $[Cu(biptpy)_2(PF_6)]$. Found: C, 56.8; H, 3.4;

N, 7.0. Calc. for $CuC_{54}H_{38}N_6P_2F_{12}\cdot1.25H_2O$: C, 56.6; H, 3.6; N, 7.3%.

The tetrafluoroborate salt was prepared in 77% yield in an analogous fashion, precipitating by addition of a saturated methanolic solution of ammonium tetrafluoroborate.

[Ru(biptpy)(tpy)][PF$_6$]$_2$

Biptpy (0.0201 g, 0.05 mmol) and [Ru(tpy)Cl$_3$] (0.0229 g, 0.05 mmol) were heated to reflux in methanol (15 cm^3) containing a few drops of 4-ethylmorpholine for 4 h. The resulting red solution was cooled and treated with saturated methanolic ammonium hexafluorophosphate. On cooling, a red solid separated and was isolated by filtration (0.031 g, 59%). IR (KBr): ν 1604s, 1450s, 1388m, 1307w, 1245m, 1164w, 840s, 790w, 767s, 732m, 698m, 559s cm^{-1}. MS (+ve FAB): m/z 334 [Ru(tpy)], 486 [Ru(biptpy)], 719 [Ru(tpy)(biptpy)], 865 [Ru(tpy)(biptpy)(PF$_6$)]. Found: C, 48.3; H, 3.0; N, 7.9. Calc. for $RuC_{42}H_{30}N_6P_2F_{12}\cdot2H_2O$: C, 48.2; H, 3.3; N, 8.0%. UV–Vis (MeCN): λ_{max} (ε) 231 (28 000), 272 (35 000), 283 (32 000), 308 (54 000), 329 (35 000), 484 nm (17 000 cm^{-1} mol^{-1}). ^{1}H NMR (CD$_3$CN, 250 MHz, 298 K): δ 9.06 (2H, s, H3′), 8.75 (2H, d, J = 8.1 Hz, H3′tpy), 8.66 (2H, d, J = 7.8 Hz, H3), 8.50 (2H, d, J = 7.1 Hz, H3tpy), 8.41 (1H, t, J = 8.0 Hz, H4′tpy), 8.32 (2H, d, J = 8.7 Hz, Ha), 8.06 (2H, d, J = 8.7 Hz, Hb), 7.97–7.89 (4H, m, H4,4tpy), 7.86 (2H, d, J = 7.0 Hz, H*o*), 7.59 (2H, d, J = 7.0 Hz, H*m*), 7.50 (1H, t, J = 7.0 Hz, H*p*), 7.43 (2H, d, J = 5.0 Hz, H6tpy), 7.35 (2H, d, J = 4.7 Hz, H6), 7.17 (4H, m, H5,5tpy). ^{1}H NMR (CD$_3$OD, 250 MHz, 298 K): δ 9.38 (2H, s, H3′), 9.02 (2H, d, J = 8.2 Hz, H3′tpy), 8.97 (2H, d, J = 7.9 Hz, H3/3tpy), 8.77 (2H, d, J = 7.9 Hz, H3/3tpy), 8.35 (1H, t, J = 8.1 Hz, H4′tpy), 8.47 (2H, d, J = 8.7 Hz, Ha/b), 8.04 (6H, m, Ha/b,4,4tpy), 7.87 (2H, dd, J = 8.4, 1.5 Hz, H*o*/*m*), 7.58 (7H, m, H*o*/*m*,*p*,6,6tpy), 7.32 (4H, t, J = 6.7 Hz, H5,5tpy).

The chloride salt was prepared in 53% yield in an analogous fashion, precipitating by addition of a saturated methanolic solution of lithium chloride.

[Ru(biptpy)Cl$_3$]

Biptpy (0.1008 g, 0.026 mmol) and ruthenium(III) trichloride (0.0543 g, 0.026 mmol) were heated to reflux in ethanol (25 cm^3) for 1 h to give a red solution. On cooling a red solid of [Ru(biptpy)Cl$_3$] separated and was isolated by filtration. It was washed with ice-cold ethanol and taken onto the next step without further purification (0.1427 g, 92%).

[Ru(biptpy)$_2$][PF$_6$]$_2$

Biptpy (0.0200 g, 0.05 mmol) and [Ru(biptpy)Cl$_3$] (0.0307 g, 0.05 mmol) were heated to reflux in methanol (15 cm^3) containing a few drops of 4-ethylmorpholine for 4 h. The resulting red solution was cooled and treated with saturated methanolic solution of ammonium hexafluorophosphate. On cooling, a brown solid separated and was isolated by filtration (0.0373 g, 62%). The red solid was recrystallised from acetonitrile by the slow diffusion of benzene. IR (KBr): ν 2985m, 2939m, 2726m, 2692m, 2596w, 1616m, 1605m, 1469m, 1430w, 1110s, 921w, 833s, 771w, 559s cm^{-1}. MS (+ve FAB): m/z 486 [Ru(biptpy)], 872 [Ru(biptpy)$_2$], 1017 [Ru(biptpy)$_2$(PF$_6$)]. Found: C, 56.4; H, 3.5; N, 6.9. Calc. for $RuC_{54}H_{38}N_6P_2F_{12}\cdot0.25C_6H_6$: C, 56.4; H, 3.4; N, 7.1%. UV–Vis (MeCN): λ_{max} (ε) 238 (66 000), 279 (100 000), 314 (110 000), 494 (45 000 cm^{-1} mol^{-1}). ^{1}H NMR (CD$_3$CN, 250 MHz, 298 K): δ 9.09 (2H, s, H3′), 8.70 (2H, d, J = 8.2 Hz, H3), 8.32 (2H, d, J = 8.7 Hz, Ha/b), 8.05 (2H, d, J = 8.4 Hz, Ha/b), 7.97 (2H, td, J = 1.5, 7.9 Hz, H4), 7.86 (2H, d, J = 6.9 Hz, H*o*/*m*), 7.52 (3H, m, H*o*/*m*,*p*), 7.46 (2H, d, J = 4.1 Hz, H6), 7.20 (2H, ddd, J = 7.9, 5.8, 1.5 Hz, H5). ^{1}H NMR (CD$_3$OD, 250 MHz, 298 K): δ 9.35 (2H, s, H3′), 8.92 (2H, d, J = 7.8 Hz, H3), 8.42 (2H, d, J = 8.7 Hz, Ha/b), 8.04 (4H, m, H4,a/b), 7.82 (2H, dd, J = 1.5, 8.4 Hz, H*o*/*m*), 7.58 (4H, m, Ha/b,6), 7.46 (1H, m, H*p*), 7.29 (2H, ddd, J = 7.6, 5.8, 1.5 Hz, H5).

The chloride salt was prepared in 54% yield in an analogous fashion, precipitating by addition of a saturated methanolic solution of lithium chloride, and the tetrafluoroborate salt prepared in 58% yield by addition of a saturated methanolic solution of ammonium tetrafluoroborate.

[Zn(biptpy)$_2$][PF$_6$]$_2$

Biptpy (0.0200 g, 0.05 mmol) and zinc(II) acetate (0.0057 g, 0.026 mmol) were heated to reflux in methanol (15 cm^3) for 12 h. The resulting clear solution was cooled and treated with saturated methanolic ammonium hexafluorophosphate. On cooling, a cream solid separated and was isolated by filtration (0.0184 g, 63%). IR (KBr): ν 1604s, 1573s, 1477s, 1427s, 836s, 794s, 767s, 559s cm^{-1}. MS (+ve FAB): m/z 834 [Zn(biptpy)$_2$], 979 [Zn(biptpy)$_2$(PF$_6$)]. Found: C, 55.9; H, 3.4; N, 7.1. Calc. for $ZnC_{54}H_{38}N_6P_2F_{12}\cdot2H_2O$: C, 55.8; H, 3.6; N, 7.2%. ^{1}H NMR (CD$_3$CN, 250 MHz, 298 K): δ 9.05 (2H, s, H3′), 8.75 (2H, d, J = 8.1 Hz, H3), 8.33 (2H, d, J = 8.8 Hz, Ha/b), 8.19 (2H, td, J = 7.5, 1.5 Hz, H4), 8.05 (2H, d, J = 8.7 Hz, Ha/b), 7.85 (4H, m, H6, *o*/*m*), 7.61 (3H, m, H,*o*/*m*), 7.42 (2H, ddd, J = 7.6, 5.2, 1.2 Hz, H5). UV–Vis (MeOH): λ_{max} (ε) 238 (67 000), 285 (63 000), 336 nm (83 000 cm^{-1} mol^{-1}).

The tetrafluoroborate salt was prepared in 69% yield in an analogous fashion, precipitating by addition of a saturated ethanolic solution of ammonium tetrafluoroborate.

[Cd(biptpy)$_2$][PF$_6$]$_2$

Biptpy (0.020 g, 0.05 mmol) cadmium(II) acetate (0.007 g, 0.026 mmol) were heated to reflux in methanol (15 cm^3) for 12 h. The resulting colourless solution was cooled and treated with saturated methanolic ammonium hexafluorophosphate. On cooling, a cream solid precipitated and was isolated by filtration (0.042 g, 72%). IR (KBr): ν 1600m, 1477m, 840s, 794m, 767m, 559m cm^{-1}. MS (+ve FAB): m/z 882 [Cd(biptpy)$_2$], 1029 [Cd(biptpy)$_2$(PF$_6$)]. Found: C, 53.1; H, 3.3; N, 7.1. Calc. for $CdC_{54}H_{38}N_6P_2F_{12}\cdot2.5H_2O$: C, 53.2; H, 3.6; N, 6.9%. ^{1}H NMR (CD$_3$CN, 250 MHz, 298 K): δ 9.01 (2H, s, H3′), 8.80 (2H, d, J = 8.0 Hz, H3), 8.28 (2H, d, J = 8.7 Hz, Ha/b), 8.23 (2H, td, J = 7.9, 1.5 Hz, H4), 8.10 (2H, d, J = 4.7 Hz, H6), 8.03 (2H, d, J = 8.7 Hz, Ha/b), 7.85 (2H, dd, J = 8.4, 1.5 Hz, H*o*/*m*), 7.55 (5H, m, H5, *p*,*o*/*m*). UV–Vis (MeCN): λ_{max} (ε) 236 (60 000), 285 (59 000), 326 nm (70 000 cm^{-1} mol^{-1}). UV–Vis (MeOH): λ_{max} (ε) 233 (37 000), 286 (46 000), 322 nm (36 000 cm^{-1} mol^{-1}).

The tetrafluoroborate salt was prepared in 73% in an analogous fashion, precipitating by addition of a saturated methanolic solution of ammonium tetrafluoroborate.

X-Ray crystallography

The crystallographic data for all the compounds examined are collected in Table 7.

[Co(biptpy)$_2$][PF$_6$]$_2$ and [Ni(biptpy)$_2$][PF$_6$]$_2$. Data were measured on a Siemens SMART[52] three-circle system with CCD area detector using the oil-mounting method at 180(2) K (maintained with the Oxford Cryosystems Cryostream Cooler).[53] Absorption correction by Psi-scan. The structures were solved by direct methods using SHELXS[54] (TREF).

[Co(biptpy)$_2$][PF$_6$]$_2$. Crystal character: red blocks. The crystals of the cobalt(II) complex were severely twinned, but the selected crystal had one dominant component. The data were, however, significantly contaminated by spurious reflections, which undoubtedly explains the relatively high R-value obtained. Systematic absences indicated either space group Cc or $C2/c$. The former was chosen for structure solution and shown to be correct by successful refinement. Inspection of the

Table 7 Crystallographic data and structure refinement details for $[M(biptpy)_2][X]_2$ (M = Co, Ni, Cu and Cd, X = PF_6; M = Ru and Zn, X = BF_4) and $[Ru(tpy)(biptpy)]Cl_2$

Complex	$[Co(biptpy)_2][PF_6]_2$	$[Ni(biptpy)_2][PF_6]_2$	$[Ru(biptpy)_2][BF_4]_2$	$[Cu(biptpy)_2][PF_6]_2$	$[Zn(biptpy)_2][BF_4]_2$	$[Cd(biptpy)_2][PF_6]_2$	$[Ru(tpy)(biptpy)]Cl_2$
Empirical formula	$C_{58}H_{46}CoF_{12}N_6OP_2$	$C_{54}H_{38}F_{12}N_6NiOP_2$	$C_{56.5}H_{47.5}N_{8.5}O_6B_2F_8Ru$	$C_{57.75}H_{41}CuF_{9.5}N_6O_{2.75}P_{1.62}$	$C_{58}H_{45}N_8O_{0.5}B_2F_8Zn$	$C_{115}H_{85}N_{13}O_2P_4F_{24}Cd_2$	$C_{43.75}H_{30}Cl_2N_6O_{9.75}Ru$
Formula weight	1191.88	1135.55	1216.22	1157.33	1101.01	2485.64	967.71
Temperature	180(2) K	180(2) K	173(2) K	173(2) K	173(2) K	173(2) K	173(2) K
Crystal system	Monoclinic	Orthorhombic	Monoclinic	Monoclinic	Triclinic	Triclinic	Monoclinic
Space group	*Cc*	*Pbam*	$P2_1/a$	*Cc*	$P\bar{1}$	$P\bar{1}$	*P*21/*c*
Unit cell dimensions *a*	22.6852(17) Å	16.5047(4) Å	15.975(1) Å	42.3037(14) Å	9.289(1) Å	13.8647(2) Å	8.8254(2) Å
b	16.9553(13) Å	17.1444(4) Å	16.982(1) Å	17.2228(6) Å	13.688(1) Å	18.7207(2) Å	20.4755(6) Å
c	16.2765(12) Å	20.3835(2) Å	20.326(1) Å	16.6487(5) Å	20.278(1) Å	21.8506(3) Å	24.0872(8) Å
α	90°	90°	90°	90°	97.01(1)°	98.3451(8)°	90°
β	120.6580(10)°	90°	93.40(1)°	108.907(2)°	99.50(1)°	98.9202(5)°	93.3490(10)°
γ	90°	90°	90°	90°	93.07(1)°	107.1244(6)°	90°
Volume	5385.4(7) Å^3	5767.8(2) Å^3	5504.5(5) Å^3	11475.6(7) Å^3	2516.8(4) Å^3	5244.01(12) Å^3	4345.2(2) Å^3
Z	4	4	4	8	2	2	4
Absorption coefficient	0.467 mm^{-1}	0.472 mm^{-1}	0.371 mm^{-1}	0.504 mm^{-1}	0.568 mm^{-1}	0.569 mm^{-1}	0.548 mm^{-1}
Crystal size	0.25 × 0.15 × 0.06 mm	0.36 × 0.24 × 0.04 mm	0.25 × 0.15 × 0.15 mm	0.25 × 0.25 × 0.25 mm	0.40 × 0.08 × 0.08 mm	0.30 × 0.30 × 0.30 mm	0.20 × 0.20 × 0.40 mm
Reflections collected	10476	21595	32250	69889	17830	231224	89452
Independent reflections	5068 [*R*(int) = 0.1499]	3642 [*R*(int) = 0.1410]	12528 [*R*(int) = 0.0406]	13604 [*R*(int) = 0.110]	11395 [*R*(int) = 0.0517]	31846 [*R*(int) = 0.083]	10331 [*R*(int) = 0.141]
Data/restraints/parameters	5068/8/721	3642/25/402	12528/12/751	13604/2/1421	11395/40/785	31846/6/1436	10331/0/552
Goodness-of-fit on F^2	0.974	1.770	1.069	1.334	1.027	1.011	1.046
Final *R* indices [$I > 2\sigma(I)$]	*R*1 = 0.0795, *wR*2 = 0.1555	*R*1 = 0.1243, *wR*2 = 0.3072	*R*1 = 0.0586, *wR*2 = 0.1566	*R*1 = 0.1486, *wR*2 = 0.3650	*R*1 = 0.0725, *wR*2 = 0.1345	*R*1 = 0.0643, *wR*2 = 0.1221	*R*1 = 0.1081, *wR*2 = 0.2243
R indices (all data)	*R*1 = 0.1714, *wR*2 = 0.1958		*R*1 = 0.0784, *wR*2 = 0.1667	*R*1 = 0.2597, *wR*2 = 0.4256	*R*1 = 0.1332, *wR*2 = 0.1566	*R*1 = 0.1445, *wR*2 = 0.1513	*R*1 = 0.2233, *wR*2 = 0.2743
Largest diff. peak and hole	0.394 and −0.358 e Å^{-3}	0.771 and −0.651 e Å^{-3}	1.164 and −0.607 e Å^{-3}	2.898 and −0.774 e Å^{-3}	0.894 and −0.600 e Å^{-3}	0.845 and −0.867 e Å^{-3}	0.949 and −1.232 e Å^{-3}

final structure did not reveal any additional symmetry. The asymmetric unit includes one molecule of tetrahydrofuran. The absolute structure of the individual crystal chosen was checked by refinement of a delta-f″ multiplier. Absolute structure parameter $x = 0.10(4)$. This gives a rather weak indication that the absolute structure is correct. Floating origin constraints were generated automatically. Refinement used SHELXL96.[55]

$[Ni(biptpy)_2][PF_6]_2$. Crystal character: yellow-orange plates. The crystals tend to be twinned, but the crystal used was primarily a single component. Systematic absences indicated either space group *Pbam* or *Pba*2. The second was chosen initially, and the structure solved. Inspection revealed the presence of mirror symmetry and the structure was transformed into *Pbam*. The Ni, both P atoms and several F atoms lie on 2-fold axes. The anions show indications of severe disorder and two low-occupancy F atoms and a number of partial occupancy solvent atoms were added to compensate for this and for a disordered solvent molecule (possibly ether). The P–F and F···F distances were constrained to standard values. The relatively high final *R*-value is readily understandable in the light of the partial twinning and the severe disorder. Refinement used SHELXTL.[56]

$[Cd(biptpy)_2][PF_6]_2$, $[Zn(biptpy)_2][BF_4]_2$, $[Ru(biptpy)_2][BF_4]_2$, $[Cu(biptpy)_2][PF_6]_2$ and $[Ru(tpy)(biptpy)]Cl_2$. Data were measured using a Nonius Kappa CCD diffractometer. Data were collected and processed with the HKL package of programs.[57] The cadmium and $Ru(biptpy)_2$ complexes were solved with SHELXS-97[58] and the zinc, copper and Ru(tpy)(biptpy) complexes with SIR92.[59] The structures were refined by full-matrix least squares on F^2 with the SHELXL-97 programs.[58] The SIR92 and SHELX-97 programs were used within the WinGX suite of programs.[60] Absorption correction for the cadmium, zinc and $Ru(biptpy)_2$ complexes was done using SORTAV[61] but the HKL package produced better data in these structures. The HKL package was used in final refinements of all the structures.

The cadmium complex $[Cd(biptpy)_2][PF_6]_2$ crystallised with benzene and nitromethane solvent molecules and the zinc complex $[Zn(biptpy)_2][BF_4]_2$ with acetonitrile and water. In the case of the cadmium complex the nitromethane solvent molecule was disordered over two sites; it was refined isotropically with geometrical restraints. In the zinc complex both BF_4 anions were also disordered over two sites. Geometrical restraints were used for the BF_4 tetrahedra. In the zinc complex, a water molecule was located (hydrogen atoms not located).

The $[Ru(biptpy)_2][BF_4]_2$ complex crystallised with nitromethane and water solvent molecules. Only the solvent molecules were disordered. One nitromethane is on a mirror plane. The second and third nitromethane molecules are disordered over two sites (refined isotropically with geometrical restraints). One water molecule is disordered over four sites.

The copper complex $[Cu(biptpy)_2][PF_6]_2$ crystallised with nitromethane, methanol and benzene solvent molecules. The crystal quality was poor and the poor final *R*-value is attributed to the weak reflection data ($R_{int} = 0.125$, $R_{sig} = 0.23$) and disorder of anions and solvent molecules. One of the PF_6 anions was disordered over two sites. In the other PF_6 anion one fluorine atom was divided over two sites. Geometrical restraints were used to keep P–F distances chemically reasonable. The nitromethane molecule situated on a mirror plane was disordered over two sites. A benzene molecule was found on a symmetry element. The methanol molecule was found and refined with population parameter of 0.5.

In the ruthenium mixed ligand complex, $[Ru(tpy)(biptpy)]Cl_2$, the crystal quality was also poor and the solvent molecules extremely disordered. Solvent electron density was spread around the Ru(II) complex and could not be identified as separate molecules, having many short contacts. All solvent peaks were refined as oxygen atoms with population parameters chosen to create reasonable temperature factors (<0.2).

CCDC reference number 186/1899.

See http://www.rsc.org/suppdata/dt/b0/b000871k/ for crystallographic files in .cif format.

Acknowledgements

We thank the EPSRC (C. L. P.; P. R. B.; J. H. GR/L91788) and the Finnish Ministry of Education (P. S.) for support, the Royal Society for the purchase of the electrochemical workstation (M. J. H.) and the EPSRC and Siemens Analytical Instruments for grants in support of a diffractometer (N. W. A.). We are grateful to the EPSRC National Mass Spectrometry Service Centre, Swansea for recording some of the mass spectra and acknowledge the use of the EPSRC's Chemical Database Service at Daresbury.[62]

References and notes

1 K. Kalyasundaran, *Photochemistry of Polypyridine and Porphyrin Complexes*, Academic Press, London, 1992; A. Juris, V. Balzani, F. Barigeletti, S. Campagna, P. Belser and A. Von Zelewsky, *Coord. Chem. Rev.*, 1988, **84**, 85; J. E. Moser, P. Bonnôte and M. Gratzel, *Coord. Chem. Rev.*, 1998, **171**, 245.
2 V. Balzani, S. Campagna, G. Denti, A. Juris, S. Serroni and M. Venturi, *Acc. Chem. Res.*, 1998, **31**, 26.
3 E. C. Constable, *Chem. Commun.*, 1997, 1073.
4 J.-P. Sauvage, J.-P. Collin, J.-C. Chambron, S. Guillerez and C. Coudret, *Chem. Rev.*, 1994, **94**, 993.
5 A. Von Zelewsky and P. Belser, *Chimia*, 1998, **52**, 620; P. Belser, S. Berhard, C. Blum, A. Beyeler, L. DeCola and V. Balzani, *Coord. Chem. Rev.*, 1999, **192**, 155.
6 M. Hissler, A. El-ghayoury, A. Harriman and R. Ziessel, *Angew. Chem., Int. Ed.*, 1998, **37**, 1717; A. Harriman and R. Ziessel, *Coord. Chem. Rev.*, 1998, **171**, 331.
7 M. Schutte, D. G. Kurth, M. R. Linford, H. Cölfen and H. Möhwald, *Angew. Chem., Int. Ed.*, 1998, **37**, 2891.
8 S. Kelch and M. Rehahn, *Macromolecules*, 1999, **32**, 5818.
9 M. D. Ward, *Chem. Soc. Rev.*, 1995, 121; V. Balzani and F. Scandola, *Supramolecular Photochemistry*, Ellis Horwood, Chichester, UK, 1991; V. Balzani, A. Juris, M. Venturi, S. Campagna and S. Serroni, *Chem. Rev.*, 1996, **96**, 759.
10 E. C. Constable and R.-A. Fallahpour, *J. Chem. Soc., Dalton Trans.*, 1996, 2389.
11 N. Armaroli, F. Barigelletti, G. Calogero, L. Flamigni, C. M. White and M. D. Ward, *Chem. Commun.*, 1997, 2181; M. D. Ward, C. M. White, F. Barigelletti, N. Armaroli, G. Calogero and L. Flamigni, *Coord. Chem. Rev.*, 1998, **171**, 481.
12 D. J. Hurley and Y. Tor, *J. Am. Chem. Soc.*, 1998, **120**, 2194.
13 J. L. Sessler, C. T. Brown, R. Z. Wong and T. Hirose, *Inorg. Chim. Acta*, 1996, **251**, 135.
14 P. G. Desmartin, A. F. Williams and G. Bernardinelli, *New J. Chem.*, 1995, **19**, 1109.
15 G. R. Desiraju, *Crystal Engineering: The Design of Organic Solids*, Elsevier, New York, 1989; G. R. Desiraju and A. Gavezotti, *J. Chem. Soc., Chem. Commun.*, 1989, 621; G. R. Desiraju, *Chem. Commun.*, 1997, 1475.
16 E. Ishow, A. Gourdon and J.-P. Launay, *Chem. Commun.*, 1998, 1909.
17 H. K. Yip, L. K. Cheng, K. K. Cheung and C. M. Che, *J. Chem. Soc., Dalton Trans.*, 1993, 2933.
18 W. R. McWhinnie and J. D. Miller, *Adv. Inorg. Chem. Radiochem.*, 1969, **12**, 135.
19 E. C. Constable, *Adv. Inorg. Chem. Radiochem.*, 1986, **30**, 69.
20 F. Kröhnke, *Synthesis*, 1976, 1.
21 E. C. Constable, A. M. W. Thompson, T. Cargill, D. A. Tocher and M. A. M. Daniels, *New J. Chem.*, 1992, **16**, 855.
22 M. L. Scudder, H. A. Godwin and I. G. Dance, *New J. Chem.*, 1999, **23**, 695.
23 B. Whittle, E. L. Horwood, L. H. Rees, S. R. Batten, J. C. Jeffery and M. D. Ward, *Polyhedron*, 1998, **17**, 373.
24 B. Whittle, E. L. Horwood, S. R. Batten, J. C. Jeffrey, L. H. Rees and M. D. Ward, *J. Chem. Soc., Dalton Trans.*, 1996, 4269.
25 E. C. Constable, C. E. Housecroft, M. Neuberger, A. G. Schneider and M. Zehnder, *J. Chem. Soc., Dalton Trans.*, 1997, 2427.
26 M.-C. Tse, K.-K. Cheung, M. C.-W. Chan and C.-M. Che, *Chem. Commun.*, 1998, 2295.

27 Only long face–edge interactions (H · · · centroid > 3.5 Å) are observed between the chains and between the planes.
28 F. Takusagawa, P. G. Yohannes and K. Mertes, *Inorg. Chim. Acta*, 1986, **114**, 165.
29 W. Henke and S. Kremer, *Inorg. Chim. Acta*, 1982, **65**, L115.
30 E. N. Maslen, C. L. Raston and A. H. White, *J. Chem. Soc.*, *Dalton Trans.*, 1974, 1803.
31 C. L. Raston and A. H. White, *J. Chem. Soc.*, *Dalton Trans.*, 1976, 7.
32 B. N. Figgis, E. S. Kucharski and A. H. White, *Aust. J. Chem.*, 1983, **36**, 1527.
33 B. N. Figgis, E. S. Kucharski and A. H. White, *Aust. J. Chem.*, 1983, **36**, 1537.
34 E. C. Constable, J. Lewis, M. C. Liptrot and P. R. Raithby, *Inorg. Chim. Acta*, 1990, **178**, 47.
35 See for example K. Lashgari, M. Kritikos, R. Norrestam and T. Norrby, *Acta Crystallogr.*, *Sect. C*, 1999, **55**, 64; M. Beley, J.-P. Collin, R. Louis, B. Metz and J.-P. Sauvage, *J. Am. Chem. Soc.*, 1991, **113**, 8521; K. L. Bushell, S. M. Couchman, J. C. Jeffery, L. H. Rees and M. D. Ward, *J. Chem. Soc.*, *Dalton Trans.*, 1998, 3397; M. Ziegler, V. Monney, H. Stoeckli-Evans, A. Von Zelewsky, I. Sasaki, G. Dupic, J.-C. Daran and G. A. Balavoine, *J. Chem. Soc.*, *Dalton Trans.*, 1999, 667.
36 The structure of a dimetallic cadmium(II) double-helical complex of 2,2′;6′,2″;6″,2‴;6‴,2⁗;6⁗,2⁗′-sexipyridine has been reported: E. C. Constable, M. D. Ward and D. A. Tocher, *J. Chem. Soc.*, *Dalton Trans.*, 1991, 1675. A mono-terpyridyl complex [Cd(tpy)-{Mn(CO)$_5$}$_2$] has been characterised: W. Clegg and P. J. Wheatley, *J. Chem. Soc.*, *Dalton Trans.*, 1973, 190. We have recently crystallographically characterised a cadmium complex of the tris-pyridyl ligand 4-thiomethyl-6-(3″-pyridyl)-2,2′-bipyridine: M. J. Hannon, C. L. Painting and W. Errington, *Chem. Commun.*, 1997, 307.
37 E. C. Constable, M. Neuberger, D. R. Smith and M. Zehnder, *Inorg. Chim. Acta*, 1998, **275**–**6**, 359.
38 E. C. Constable, R. Martinez-Manez, A. M. W. Cargill Thompson and J. V. Walker, *J. Chem. Soc.*, *Dalton Trans.*, 1994, 1585.
39 E. C. Constable, P. Haverson, D. R. Smith and L. Whall, *Polyhedron*, 1997, **16**, 3615.
40 J. M. Rao, D. J. Macero and M. C. Hughes, *Inorg. Chim. Acta*, 1980, **41**, 221.
41 E. C. Constable and A. M. W. Cargill Thompson, *J. Chem. Soc.*, *Dalton. Trans.*, 1994, 1409.
42 M. Maestri, N. Armaroli, V. Balzani, E. C. Constable and A. M. W. Cargill Thompson, *Inorg. Chem.*, 1995, **34**, 2759.
43 D. K. Liu, B. S. Brunschwig, C. Creutz and N. Sutin, *J. Am. Chem. Soc.*, 1986, **108**, 1750.
44 G. Albano, V. Balzani, E. C. Constable, M. Mastri and D. R. Smith, *Inorg. Chim. Acta*, 1998, **277**, 225.
45 K.-Y. Ho, W.-Y. Yu, K.-K. Cheung and C.-M. Che, *J. Chem. Soc.*, *Dalton Trans.*, 1999, 1581.
46 J.-P. Collin, I. M. Dixon, J.-P. Sauvage, J. A. G. Williams, F. Barigelletti and L. Flamigni, *J. Am. Chem. Soc.*, 1999, **121**, 5009.
47 K.-Y. Ho, W.-Y. Yu, K.-K. Cheung and C.-M. Che, *Chem. Commun.*, 1998, 2101.
48 The spike on the solid state luminescence spectrum is scattered light.
49 M. J. Hannon, C. L. Painting and W. Errington, *Chem. Commun.*, 1997, 307; M. J. Hannon, C. L. Painting and W. Errington, *Chem. Commun.*, 1997, 1805.
50 S. Weidner and Z. Pikramenou, *Chem. Commun.*, 1998, 1473; M. Chavarot and Z. Pikramenou, *Tetrahedron Lett.*, 1999, **40**, 6865.
51 J. N. Demas and G. A. Crosby, *J. Phys. Chem.*, 1971, **75**, 991.
52 *SMART User's manual*, Siemens Industrial Automation Inc, Madison, WI, 1994.
53 J. Cosier and A. M. Glazer, *J. Appl. Crystallogr.*, 1986, **19**, 105.
54 G. M. Sheldrick, *Acta Crystallogr.*, *Sect. A*, 1990, **46**, 467.
55 G. M. Sheldrick, SHELX-96 (beta-test) (including SHELXS and SHELXL), University of Göttingen, 1996.
56 G. M. Sheldrick, SHELXTL Ver. 5.1, Bruker Analytical X-Ray Systems, Madison, WI, 1997.
57 Z. Otwinowski and W. Minor, *Methods Enzymol.*, 1997, **276**, 307.
58 G. M. Sheldrick, SHELX-97: Programs for Crystal Structure Analysis (Release 97-2), Institüt für Anorganische Chemie der Universität, Tammanstrasse 4, D-3400 Göttingen, Germany, 1998.
59 A. Altomare, G. Cascarano, C. Giacovazzo and A. Guagliardi, *J. Appl. Crystallogr.*, 1993, **26**, 343.
60 L. J. Farrugia, WinGX: A Windows Program for Crystal Structure Analysis, University of Glasgow, 1998.
61 R. H. Blessing, *Acta Crystallogr.*, *Sect. A*, 1995, **51**, 33; R. H. Blessing, *J. Appl. Crystallogr.*, 1997, **30**, 421.
62 D. A. Fletcher, R. F. McMeeking and D. Parkin, *J. Chem. Inf. Comput. Sci.*, 1996, **36**, 746; F. H. Allen and O. Kennard, *Chem. Des. Automat. News*, 1993, **8**, 1 and 31.
63 NMR software manual, Bruker analytik GmbH, 1997.
64 GPES for windows, version 4.2, Eco Chemie B.V., Utrecht, The Netherlands, 1995.
65 Felix Software, version 1.1, Photon Technology International Inc., Brunswick, USA, 1996.